Accuracy of density functional theory in predicting formation energies of ternary oxides from binary oxides and its implication on phase stability

Citation: Hautier, Geoffroy et al. "Accuracy of Density Functional Theory in Predicting Formation Energies of Ternary Oxides from Binary Oxides and Its Implication on Phase Stability." Physical Review B 85.15 (2012). ©2012 American Physical Society

As Published: http://dx.doi.org/10.1103/PhysRevB.85.155208

Publisher: American Physical Society

Persistent URL: http://hdl.handle.net/1721.1/71707

Version: Final published version: final published article, as it appeared in a journal, conference proceedings, or other formally published context

PHYSICAL REVIEW B **85**, 155208 (2012)

Accuracy of density functional theory in predicting formation energies of ternary oxides from binary oxides and its implication on phase stability

Geoffroy Hautier,[*] Shyue Ping Ong, Anubhav Jain, Charles J. Moore, and Gerbrand Ceder[†]
Massachusetts Institute of Technology, Department of Materials Science and Engineering, 77 Massachusetts Avenue,
02139 Cambridge, Massachusetts, USA

(Received 6 January 2012; published 30 April 2012)

The evaluation of reaction energies between solids using density functional theory (DFT) is of practical importance in many technological fields and paramount in the study of the phase stability of known and predicted compounds. In this work, we present a comparison between reaction energies provided by experiments and computed by DFT in the generalized gradient approximation (GGA), using a Hubbard U parameter for some transition metal elements (GGA + U). We use a data set of 135 reactions involving the formation of ternary oxides from binary oxides in a broad range of chemistries and crystal structures. We find that the computational errors can be modeled by a normal distribution with a mean close to zero and a standard deviation of 24 meV/atom. The significantly smaller error compared to the more commonly reported errors in the formation energies from the elements is related to the larger cancellation of errors in energies when reactions involve chemically similar compounds. This result is of importance for phase diagram computations for which the relevant reaction energies are often not from the elements but from chemically close phases (e.g., ternary oxides versus binary oxides). In addition, we discuss the distribution of computational errors among chemistries and show that the use of a Hubbard U parameter is critical to the accuracy of reaction energies involving transition metals even when no major change in formal oxidation state is occurring.

DOI: 10.1103/PhysRevB.85.155208 PACS number(s): 71.15.Mb

I. INTRODUCTION

Density functional theory (DFT) computations can provide the total energy of solid compounds. These total energies are then used to obtain reaction energies which are of importance in many fields such as batteries, hydrogen storage, Hg absorption, carbon capture, or thermochemical water splitting.[1–8] Reaction energies are also critical to the *ab initio* study of the thermodynamic stability of known materials[9–14] or the prediction of novel phases.[15–27] Indeed, it is a compound's energy relative to the energy from combinations of other phases, which determines its stability.

While comparisons between experimental and computed energies of reactions for solids exist in the literature, they tend to focus on very specific chemistries and/or crystal structures (e.g., perovskites[28,29]). In contrast to the evaluation of molecular systems in the quantum chemistry field,[30,31] there is a lack of statistically broad studies on the accuracy of specific DFT functionals in predicting energies of reactions between solid phases. This situation makes it difficult to add an error bar to predictions of reaction energies and can hinder the evaluation of the results provided by *ab initio* phase stability studies (i.e., the study of phase diagrams built from *ab initio* computations). Hence, the objective of this paper is to assess the accuracy of DFT in predicting reaction energies relevant to phase stability in multicomponent oxides by comparing, on a large data set, experimental and computed reaction energies from binary oxides to ternary oxides.

Our comparison between DFT and experimental reaction energies is mainly based on two very large experimental thermochemical data sources, the Kubachewski and the NIST databases.[32,33] While it is common to report reaction energies from the elements, elemental reaction energies are not, in general, relevant to phase stability. Indeed, when one wants to determine if a predicted multicomponent compound is thermodynamically stable, the reaction energy determining the stability of the new compound is typically not with respect to the elements but to more chemically similar phases. For instance, the stability of a ternary oxide is most often determined by its relative energy versus other oxides (binaries and/or ternaries) and not versus the elements. In this work, we focus on the accuracy of the reaction energies that are relevant to the phase stability of ternary oxides with respect to binary oxides.

Using 135 of these solid phase reactions, we present in this paper the largest reported comparison between experimental and DFT computed solid phase reaction energies. We analyze the error distribution, and the chemistries for which errors are the most significant. Finally, we discuss the implication of our work on the evaluation of multicomponent phase diagrams obtained by GGA and GGA + U. We stress that our study, by providing an error distribution for reaction energies involving chemically similar compounds, can be used to quantitatively assess the results obtained when computing the stability of new predicted phases with DFT.

II. METHODOLOGY

A. DFT parameters

The DFT computations were performed using a generalized gradient approximation (GGA) functional parametrized by Perdew, Burke, and Ernzerhof (PBE).[34] The transition metals Cu, Fe, Cr, Co, Mn, Ni, V, Nb, and Mo were assigned a U parameter to correct for the self-interaction error present in GGA.[35,36] This U parameter was fitted to experimental binary oxide formation energies using the Kubaschewski tables[32] following the approach from Wang *et al.*[37] We excluded tungsten from our analysis due to the difficulty to fit a U value reproducing experimental enthalpies. All compounds were run with a k-point density of at least 500/(number of atom in unit cell) k points. The Vienna *ab initio* software package[38] (VASP) was used with the provided projector augmented wave (PAW) pseudopotentials.[39] All pseudopotentials and U values are provided in Appendix A. With these parameters, the computations are expected to be converged to one meV/atom for oxide materials.[40] More details on the high-throughput *ab initio* methodology and parameters can be found in Jain *et al.*[40] All magnetic moments were initialized in a ferromagnetic (FM) state, but compounds containing V, Mo, Cu, Nb, Co, Cr, Mn, Ni, and Fe were also computed with an antiferromagnetic (AFM) state initialization. We computed all nonsymmetrically equivalent AFM magnetic orderings in the smallest possible supercells using Hart's algorithm.[41] From all different FM and AFM initializations, the one with the lowest energy was chosen for our data set. For entries with mixed oxidation states (i.e., Fe_3O_4 and Mn_3O_4), we verified that charge ordering actually occurred in the GGA + U computation. In all cases, two full subsequent ionic relaxations were performed using the DFT parameters described above and the AFLOW wrapper around VASP.[42,43]

B. Experimental data selection

Due to their relevance in technological applications and the large experimental data set available for ternary compounds, we only considered oxides in this study. For each oxide compound in the Kubachewski tables,[32] we searched for a corresponding crystal structure in the Inorganic Crystal Structure Database (ICSD).[44] Often the crystal system (e.g., monoclinic or cubic) or the mineral name is given in the Kubachewski tables and we used this partial structure information to choose the corresponding ICSD entries among polymorphs. When the data provided by Kubachewski were not sufficient to choose among polymorphs, we chose the lowest-energy polymorph. The Kubaschewski entries that did not have a corresponding ICSD entry were disregarded, as were compounds with partial occupancies.

To exclude as much as possible unreliable experimental data from our study, we double-checked the formation enthalpies provided by Kubachewski versus other sources (the NIST database,[33] the Landolt-Bornstein database,[45] the CTDP database,[46] and the scientific literature). The principal verification was performed against the NIST database,[33] which contains less data (especially for ternary oxides) but provides more recent and accurate data than the Kubachewski tables. We found 107 oxide entries in the Kubachewski table having an equivalent entry in the NIST database. If the difference in enthalpy between the two pieces of data was higher than 5 meV/atom, we chose the NIST value. This situation occurred for 19 entries in our data and the largest differences (>30 meV/atom) were found for six entries: Mg_2TiO_5 (216 meV/atom), K_2SiO_3 (72 meV/atom), Be_2SiO_4 (43 meV/atom), and CuO (30 meV/atom). The remaining entries in Kubachewski for which no NIST data are available were compared with the information in the Landolt-Bornstein database.[45] For the entries with large discrepancies (>20 meV/atom in formation enthalpy), we looked for a third source to determine whether the value from the Kubachewski or Landolt-Bornstein database should be used. We had to exclude four compounds (Cs_2SiO_3, K_3PO_4, Li_3AsO_4, and BaV_2O_6) because of the lack of a reliable third source, and we selected the value from the Landolt database for four other compounds ($FeMoO_4$, $Na_4V_2O_7$, Na_2MoO_4, and $KFeO_2$). The remaining entries (without data in NIST and Landolt-Bornstein) were compared to the CTDP database. The eight entries in the CTDP database were all in agreement (within 20 meV/atom) with the Kubachewski data. Finally, the remaining 14 compounds (without data in NIST, Landolt-Bornstein, and CTDP) were compared to values found in the literature. Seven had to be excluded from our data set as no consistent data were found in the literature (SrB_4O_7, $LiTaO_3$, $LiNbO_3$, $LaPO_4$, LiB_3O_5, $NaVO_3$, and $CdTiO_3$)

Each enthalpy of formation in the Kubachewski table is given with an experimental error. Assuming that the experimental errors on enthalpies of formation are normally distributed and independent, the error on a reaction enthalpy (which is the result of a sum of enthalpy of formations) can be computed using the rule of summation of normally distributed random variables. The resulting error on the reaction energy is also normally distributed, with a standard deviation of $\sigma_{\text{reaction}} = \sqrt{\sum_i a_i^2 \sigma_i^2}$. The σ_i represent the standard deviation associated with the experimental enthalpy of formation of each compound involved in the reaction, and a_i are the stoichiometric coefficients associated with the product i in the reaction. For the few entries without any experimental error provided in the Kubachewski table, the Landolt database, or the literature, we attributed an error of 10 meV/atom corresponding to the average experimental error in the Kubachewski tables. We attributed an experimental error of 5 meV/atom for the more reliable NIST data.

C. Evaluating 0-K energies from 298-K enthalpies

The Kubachewski tables provide enthalpies of formation at 298 K, while the computed total energies refer to energies at 0 K. To obtain experimental enthalpies at 0 K, one needs to integrate the heat capacity between 0 and 298 K. The experimental heat capacity of each compound is often provided in thermochemical tables as a polynomial expansion on the temperature and it is tempting to directly integrate the polynomial to 0 K. However, this polynomial expansion is only valid for temperatures above 298 K. Hence, we instead fit a Debye-type equation to the heat capacity at 298 K with the additional constraint that the integration of this heat capacity divided by the temperature should give the formation entropy (also provided in the thermochemical tables) at 298 K. The heat capacity at constant pressure (c_p) and per atom of compound is assumed to follow the Debye form

$$c_p(T;T_D,A) = A\left(\frac{T}{T_D}\right)^3 \int_0^{\frac{T_D}{T}} \frac{x^4 e^x}{(e^x-1)^2}\,dx, \tag{1}$$

where T_D, the Debye temperature, and A are constants. The constants A and T_D are determined for each compound from the heat capacity at 298 K, $c_{p,298\,\text{K}}$, and the entropy at 298 K, $S_{298\,\text{K}}$, provided in the Kubachewski tables:

$$c_p(298,T_D,A) = c_{p,298\,\text{K}}, \tag{2}$$

$$\int_0^{298} \frac{c_p(T;T_D,A)}{T}\,dT = S_{298\,\text{K}}. \tag{3}$$

Integrating the Debye model in Eq. (1) with the fitted A and T_D leads to the experimental enthalpy at 0 K:

$$H_{0\,\mathrm{K}} \simeq H_{298\,\mathrm{K}} - \int_0^{298} c_p(T;T_D,A)\,dT. \qquad (4)$$

We compared our fitted Debye model to actual heat-capacity measurements down to 0 K for a few compounds, and found good agreement (see Appendix B).

As the heat-capacity integration component depends on the entropy and heat-capacity value provided by the Kubachewski tables, we compared them to the NIST database. We did not find any large differences except for the $NaAlO_2$ entropy for which we used the NIST values. For Fe_2ZnO_4, we used direct values from the heat-capacity integration provided in King *et al.*[47] as the heat capacity reported in the Kubachewski tables is unphysical and negative. In addition, we neglect the pressure times volume (PV) term, assuming that the formation *energy* at 0 K is equal to the formation *enthalpy* at 0 K. When considering reaction energies between solids, the PV term of the enthalpy is negligible. We also neglect the zero-point energy (ZPE) contribution to the energy (typically less than a few meV/atom).[48,49]

We provide in Appendix C for each compound the corresponding ICSD number, the experimental enthalpy of formation from the elements at 0 K, the experimental error, the source of the enthalpy data (Kubachewski, NIST, or Landolt) as well as the DFT (GGA and GGA + U) total energy obtained by ionic relaxation. We also provide as Supplemental Material the relaxed structures (in FM state) for each of the selected compounds to facilitate future comparison of our data set to other functionals or computational approaches.[50]

D. Reaction energy critical to phase stability

When considering an $A_xB_yC_z$ compound in an A-B-C chemical system, there are many different reaction energies forming this compound that can be defined. Most often, the formation energy from the elements (e.g., $A + B + 2C \rightarrow ABC_2$) is reported, but other reactions can be defined as well, for instance, from binaries to ternaries (e.g., $\frac{1}{2}A_2C + \frac{1}{2}B_2C_3 \rightarrow ABC_2$) or even between ternaries and binaries (e.g., $\frac{1}{5}A_5BC_4 + \frac{2}{5}B_2C_3 \rightarrow ABC_2$). In this work, we present a method to choose the reaction most relevant to phase stability for a given $A_xB_yC_z$ phase. The algorithm relies on the convex-hull construction. The convex-hull construction effectively evaluates the stability of a given compound against any linear combination of compounds that have the same averaged composition, and is the common procedure to assess if a compound is stable versus the decomposition to other products. First, we construct the convex hull with all phases existing in the A-B-C, including all elemental, binary, and ternary phases with the exception of the targeted $A_xB_yC_z$ phase. Then, we detect which phases constitute the equilibrium triangle in which the $A_xB_yC_z$ composition lies. The reaction from these phases in the equilibrium triangle to form the $A_xB_yC_z$ phase is defined as the reaction critical to phase stability. Indeed, it is this reaction that determines directly if the $A_xB_yC_z$ phase is stable (i.e., on the convex hull) or not (i.e., above the convex hull) as it compares the $A_xB_yC_z$ phase to the most competitive combination of phases. Figure 1 illustrates this algorithm for a hypothetical A-B-C system and a ABC_3 ternary phase. Using the phase diagram built by the convex-hull construction without the ABC_3 phase, we can see that the ABC_3 composition (blue dot) lies in the triangle formed by the A_2C, BC_3, and BC_2 phases (the decomposition is indicated by the blue arrows). The critical reaction energy to phase stability is therefore $\frac{1}{2}A_2C + \frac{1}{2}BC_3 + \frac{1}{2}BC_2 \rightarrow ABC_3$. While we illustrated the method by using examples from ternary phase diagrams, the algorithm is easily generalizable to higher component systems (e.g., quaternaries) by considering the relevant equilibrium simplices.

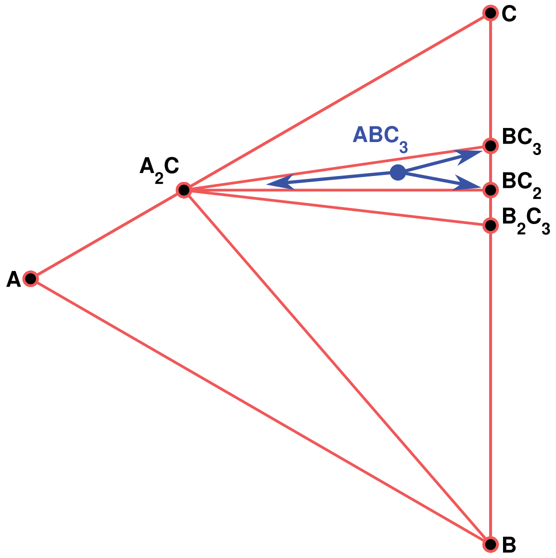

FIG. 1. (Color online) Illustration of the procedure to determine the reaction critical to phase stability for an ABC_3 compound. By building the phase diagram using the convex-hull construction on all phases in the A-B-C system with the exception of ABC_3, we find that the equilibrium triangle consists in A_2C, BC_3, and BC_2. The critical reaction energy to phase stability is therefore $\frac{1}{2}A_2C + \frac{1}{2}BC_3 + \frac{1}{2}BC_2 \rightarrow ABC_3$.

We applied this algorithm to determine what would be the critical reaction energy from binary to ternary oxides for each ternary oxide present in our data set. For chemical systems including only cations with single oxidation states, there is only one binary oxide to ternary oxide reaction that needs to be considered. For instance, in the case of $LiAlO_2$, the only reaction energy forming this ternary compound from binary oxides is $\frac{1}{2}Al_2O_3 + \frac{1}{2}Li_2O \rightarrow LiAlO_2$. On the other hand, when a ternary oxide contains elements forming in several oxidation states (e.g, $CoFe_2O_4$), there is more than one reaction involving binary oxides reacting to form the ternary compound, but only one reaction will be directly critical to the phase stability of the ternary (i.e., $CoO + Fe_2O_3 \rightarrow CoFe_2O_4$). If any of the competing phases is a gas (e.g., CO_2 for a carbonate or SO_2 for a sulfate), the ternary oxide was not considered in our data set. Gases were excluded from our analysis because of the large known errors in DFT associated with molecular species (e.g., oxygen molecule overbinding).[37,51]

In total, our data set consists of 135 reaction energies and each computed and experimental reaction energy is present in Appendix C. In this work, we will express all reaction energies as energy per atom of ternary compound (eV/atom or meV/atom); 10 meV/atom corresponds to about 1 kJ/mol-atom.

III. RESULTS

Figure 2 plots the experimental reaction energies as a function of the computed reaction energies. All reactions involve binary oxides to ternary oxides and have been chosen as presented in Sec. II. The error bars indicate the experimental error on the reaction energy. The data points follow roughly the diagonal and no computed reaction energy deviates from the experimental data by more than 150 meV/atom. Figure 2 does not show any systematic increase in the DFT error with larger reaction energies. This justifies our focus in this study on absolute and not relative errors.

In Fig. 3, we plot a histogram of the difference between the DFT and experimental reaction energies. GGA + U underestimates and overestimates the energy of reaction with the same frequency, and the mean difference between computed and experimental energies is 9.6 meV/atom. The root-mean-square (rms) deviation of the computed energies with respect to experiments is 34.4 meV/atom. Both the mean and rms are very different from the results obtained by Lany on reaction energies *from the elements*.[52] Using pure GGA, Lany found that elemental formation energies are underestimated by GGA with a much larger rms of 240 meV/atom. Our results are closer to experiments because of the greater accuracy of DFT when comparing chemically similar compounds such as binary and ternary oxides due to errors cancellation.[40] We should note that even using elemental energies that are fitted to minimize the error versus experiment in a large set of reactions, Lany reports that the error is still 70 meV/atom and much larger than what we find for the relevant reaction energies. The rms we found is consistent with the error of 3 kJ/mol-atom (30 meV/atom) for reaction energies from the binaries in the limited set of perovskites reported by Martinez *et al.*[29]

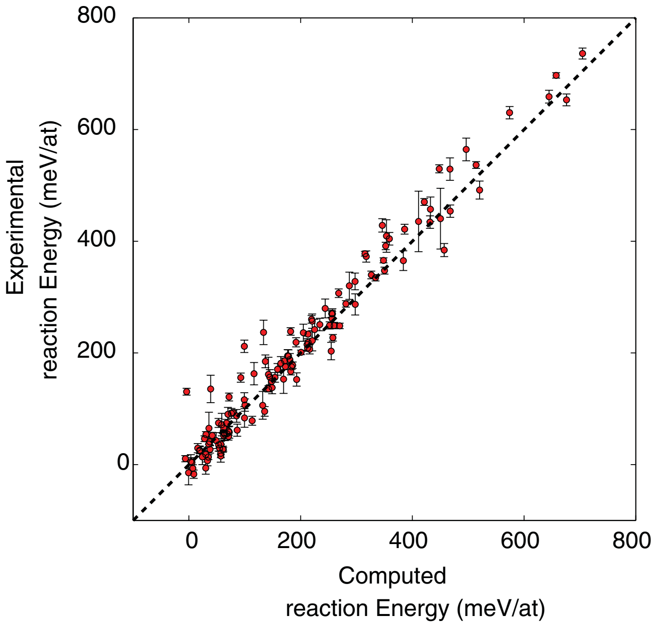

FIG. 2. (Color online) Experimental reaction energy as function of the computed reaction energy (in meV/atom). The error bar indicates the experimental error. As the reaction energies are typically negative, the graph actually plots the negative of the reaction energy.

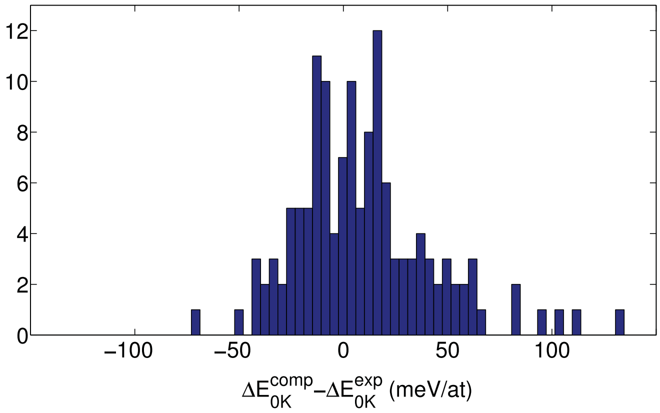

FIG. 3. (Color online) Histogram of the difference between computed ($\Delta E_{0\mathrm{K}}^{\mathrm{comp}}$) and experimental ($\Delta E_{0\mathrm{K}}^{\mathrm{expt}}$) energies of reaction (in meV/atom).

Very often, instead of the exact reaction energy, one is interested in knowing if a ternary compound is stable enough to form with respect to the binaries. This is typically the case when a new ternary oxide phase is proposed and tested for stability versus the competing binary phases.[18] From the 131 compounds for which reaction energies are negative according to experiments, all but two (Al_2SiO_5 and $CeAlO_3$) are also negative according to computations. This success in predicting stability versus binary oxides of known ternary oxides can be related to the very large magnitude of reaction energies from binary to ternary oxides compared to the typical errors observed (rms of 34 meV/atom). Indeed, for the vast majority of the reactions (109 among 131), the experimental reaction energies are larger than 50 meV/atom. It is unlikely then that the DFT error would be large enough to offset this large reaction energy and make a stable compound unstable versus the binary oxides.

The histogram in Fig. 3 shows several reaction energies with significant errors. Failures and successes of DFT are often known to be chemistry dependent, and we present the effect of the chemistry on the DFT error by plotting, in Fig. 4, a matrix of absolute reaction energies errors. The x axis represents the oxides of element A and the y axis the oxide of element B. Each element in the matrix corresponds to an A-B-O chemical system. When several reaction energies are available in a chemical systems (i.e., several ternary compounds are present), we plotted the maximum absolute error energy in this system. The matrix is symmetric as A-B-O is equivalent to B-A-O. The elements are sorted by their Mendeleev number[53] so that important chemical classes (e.g., alkalis or transition metals) are grouped together. The first row and column in the matrix indicate the mean of the difference computed experimental for one given element across all ternary oxide chemistries.

It is remarkable that no systematically larger error is present for elements with partially filled d orbitals (e.g., Fe, Mn, Co, or Ni), which indicates that the use of a Hubbard U is sufficient to compensate the error associated with the localized d orbitals. On the other hand, elements containing f electrons such as

TABLE I. Comparison between the reaction energies from binary oxides to Ce-containing ternary oxides from experiment, computed with GGA (without a U applied on the f orbitals in Ce) and with a U applied on f orbitals in Ce. The U value for Ce was not optimized and set arbitrarily to 3 eV.

Reaction	Computed energy without U on f orbitals (meV/atom)	Reaction energy with U on f orbitals (meV/atom)	Experimental energy (meV/atom)
$\frac{1}{2}$ $Ce_2O_3 + \frac{1}{2}$ $Cr_2O_3 \rightarrow CeCrO_3$	−38.9	−52.2	−135
$\frac{1}{2}$ $Ce_2O_3 + \frac{1}{2}$ $Al_2O_3 \rightarrow CeAlO_3$	4.19	−50.9	−130

cerium show very large deviations from experiments. Both reaction energies involving cerium (i.e., related to $\frac{1}{2}$ $Ce_2O_3 + \frac{1}{2}$ $Cr_2O_3 \rightarrow CeCrO_3$ and $\frac{1}{2}$ $Ce_2O_3 + \frac{1}{2} Al_2O_3 \rightarrow CeAlO_3$) disagree by extremely large values (around 130 meV/atom) from the experimental data. We should note that, in this study, we did not use any U value on f orbitals and those Ce^{3+} compounds have a $4f^1$ electronic configuration with one f electron participating in the bonding. This f electron is poorly represented by GGA as Ce_2O_3, $CeCrO_3$ and $CeAlO_3$ are computed to be metallic while they are in reality insulators. It is likely that this incorrect representation of the electronic structure explains the large discrepancy obtained in reaction energies for Ce^{3+} oxides. The difficulty to correctly model the electronic structure of Ce_2O_3 with GGA had already been pointed out by Skorodumova *et al.*[54] One proposed solution has been to apply a Hubbard U on the cerium f electrons.[55] While fitting a U value for Ce is beyond the scope of this work, we indeed observe the reaction energy getting closer to the experimental data by applying a moderate U value (U = 3 eV) on the f electrons in Ce for both $CeCrO_3$ and $CeAlO_3$ (see Table I). The other f-containing elements (i.e., U and La) do not show as large discrepancies as Ce (with the exception of one uranium-based compound Cs_2UO_4). This observation can be easily rationalized by the nonoccupied character of the f orbitals in the specific oxidation states of these uranium and lanthanum compounds (i.e., U^{6+} and La^{3+} do not have any occupied f-electron states).

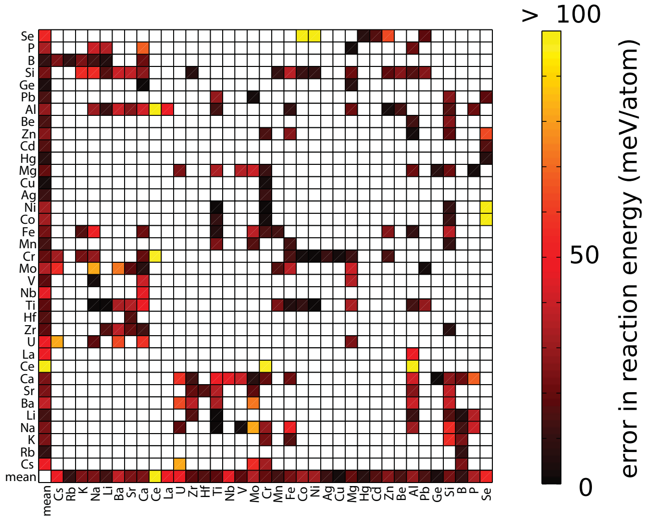

FIG. 4. (Color online) Matrix of the difference between computed and experimental energies of reaction ($|\Delta E_{0\,\mathrm{K}}^{\mathrm{comp}} - \Delta E_{0\,\mathrm{K}}^{\mathrm{expt}}|$). The x (y) axis represents the oxides of element A (B). Each element in the matrix corresponds to a chemical system A-B-O. When several reaction energies are available in a chemical systems (i.e., several ternary compounds are present), we plot the maximum absolute error energy in this system. The matrix is symmetric as A-B-O is equivalent to B-A-O. The elements are sorted by Mendeleev number and the first row indicates the mean of the difference across the different chemistries.

Another chemistry-dependent effect is the importance of a relativistic treatment, as effects due to spin-orbit coupling will be larger for heavier elements (e.g., Pb). Recently, Ahuja *et al.* showed that spin-orbit coupling is required to accurately reproduce certain reaction energies in lead-containing compounds.[56] The reaction energies studied by Ahuja *et al.* involved a metal and two oxides with different oxidation states. Our simpler reactions (involving only oxides in a Pb^{2+} oxidation state) do not show major errors with lead-containing compounds (see Fig. 4 and Table II). We should note, however, that spin-orbit coupling is incorporated indirectly in our computations in the construction of the PAW pseudopotentials.

Two molybdenum-based compounds ($BaMoO_4$ and $Na_2Mo_2O_7$) also show large errors (−72.9 and 82.2 meV/atom). While the thermochemical data for both these compounds is consistent in the Kubachewski and Landolt databases, a more refined literature search indicated that the discrepancy is due to measurements errors for both databases. The formation energy from the elements for $Na_2Mo_2O_7$ is reported from two different methods at −2245 and −2248.5 kJ/mol,[57,58] while the Kubachewski data report −2361 kJ/mol. Similarly, three literature references indicate a value around −1546 kJ/mol for the formation energy from the elements for $BaMoO_4$,[59–61] in contradiction with the value in the Kubachewski of −1516.3 kJ/mol. For both compounds, these revised values from the literature lead to closer agreement with the computed data (respectively, −26 and −22 meV/atom differences). Some selenate compounds in our data set show large deviations as well. The discrepancies are especially large for $NiSeO_3$ and $CoSeO_3$ (respectively, 113 and 105 meV/atom), but also for $ZnSeO_3$ (63 meV/atom). The three other selenate compounds ($HgSeO_3$, $PbSeO_3$, and $CdSeO_3$) do not show unusual errors. After a more detailed study, we found that Olin considered both experimental results from Ni and Co uncertain enough to exclude them from his comprehensive review on selenates.[62] Olin confirms, on the other hand, the value provided by Kubachewski for $ZnSeO_3$. Finally, a surprising large discrepancy is present for $Ca_3(PO_4)_2$ (67.9 meV/atom) and further investigation in the literature showed that the $Ca_3(PO_4)_2$ composition forms two polymorphs: an α and β phase. Both phases form in the rhombohedral crystal system and can not be discriminated from the information present in the Kubachewski tables, but enthalpy data from another source showed that the enthalpy

TABLE II. Experimental and computed reaction energies for lead-containing compounds.

Reaction	Computed (meV/atom)	Experimental (meV/atom)	Difference (meV/atom)
$TiO_2 + PbO \rightarrow PbTiO_3$	−36	−65	29
$SeO_2 + PbO \rightarrow PbSeO_3$	−177	−195	18
$MoO_3 + PbO \rightarrow MoPbO_4$	−154	−156	2
$SiO_2 + PbO \rightarrow PbSiO_3$	−55	−29	25
$SiO_2 + 2PbO \rightarrow Pb_2SiO_4$	−37	−40	3

provided by Kubachewski most likely relates to the β phase.[63] In our work, we selected the α phase because of the absence of crystallographic data with full occupancies for the β phase in the ICSD. By using a simple ordering algorithm combined with an electrostatic energy model to select an ordering,[41] we estimate the β phase to be 32 meV/atom lower in energy than the α phase. Using the ordered β phase, the computed value is in better agreement with experiment (35.9 meV/atom difference).

Our data can be used to fit a probability distribution of the DFT errors. The simplest model would be to consider that the computational error is distributed normally with mean μ and standard deviation σ. Some of the large outliers discussed previously (i.e., $BaMoO_4$, $Na_2Mo_2O_7$, $Ca_3(PO_4)_2$, and the nickel and cobalt selenates) are due to errors external to DFT (inaccurate enthalpy measurements or structure assignment), and we will exclude them for the rest of the analysis. Likewise, we excluded the cerium-based compounds as those errors could likely be fixed by using an adequate U value on f electrons. In addition, the Kubachewski tables provide for each enthalpy of formation an estimate of the experimental accuracy of the measurement that needs to be deconvoluted from the error due to DFT. The difference between experimental and computed energy for a reaction i can be represented by a random variable X_i, that is the sum of the experimental error X_i^{expt} and the DFT error X_i^{DFT}:

$$X_i = X_i^{\text{expt}} + X_i^{\text{DFT}}. \tag{5}$$

Assuming that the experimental error for the reaction i is distributed normally with zero mean and a standard deviation equal to σ_i (computed from the error bar on the formation energy of all compounds participating in the reaction as presented in Sec. II) and that the error between DFT and experiment is distributed normally as well with a mean μ and a standard deviation σ, we can show that

$$\begin{aligned} X_i &= N(0,\sigma_i) + N(\mu,\sigma) && (6)\\ &= N\left(\mu,\sqrt{\sigma^2+\sigma_i^2}\right) && (7)\\ &= \frac{1}{\sqrt{2\pi\left(\sigma^2+\sigma_i^2\right)}} e^{-\frac{(x_i-\mu)^2}{2(\sigma^2+\sigma_i^2)}}. && (8)\end{aligned}$$

The unknown parameters to evaluate are the mean and standard deviation of the DFT error (μ and σ). These two parameters can be estimated by a maximum likelihood approach.[64] The log-likelihood L for the n observations (i.e., the n reaction energies) can be expressed as

$$\begin{aligned} L &= \ln\left(\prod_{i=1}^{n} p(X_i = x_i)\right) && (9)\\ &= \sum_{i=1}^{n} -\frac{(x_i-\mu)^2}{2\left(\sigma^2+\sigma_i^2\right)} - \frac{1}{2}\sum_{i=1}^{n} \ln\left[2\pi\left(\sigma^2+\sigma_i^2\right)\right]. && (10)\end{aligned}$$

Maximizing the log-likelihood can be performed by searching for μ^* and σ^* such that $\frac{\partial}{\partial\mu}L = 0$ and $\frac{\partial}{\partial\sigma}L = 0$. In the case with no experimental error ($\sigma_i = 0$), we find the well-known mean and standard deviation maximum likelihood estimates: $\mu^* = \frac{1}{n}\sum_{i=1}^{n} x_i$ and $\sigma^* = \frac{1}{n}\sum_{i=1}^{n}(x_i - \mu^*)^2$.

Searching for μ^* and σ^* numerically, we found a mean estimate of 5.6 ± 4.6 meV/atom and a standard deviation estimate of 24 ± 3.5 meV/atom. The 95% percent confidence intervals have been evaluated using Fischer's information matrix.[65] From this normal model of the DFT error, we see that 90% of the errors should lie within ±40 meV/atom, providing a reasonable order of magnitude for an "error bar" around the oxides reactions energies relevant for phase stability.

Reaction energies involving a change in oxidation states are expected to be more difficult to model using DFT. In our data set, only three reactions (shown in Table III) involve a change in formal oxidation state (as defined in the ICSD). While the data set is too small to draw any strong conclusion, the few reaction energies involving a change in oxidation states do not show larger errors than the typical errors found for the entire data set.

It has been demonstrated that GGA + U is required to accurately predict the reaction energies of transition metal oxides when a change in oxidation state is involved (redox reactions).[37,51] As most reaction energies studied in this work do not involve changes in oxidation state, it is of interest to probe if the Hubbard U parameter is beneficial to the accuracy of reaction energies. Therefore, for all reactions involving at least one element requiring a U value (see Sec. II), we also computed the GGA (without U) reaction energy and compared the distribution of errors in the two data sets (GGA and GGA + U). Applying the previously presented maximum likelihood estimation for both samples (GGA and GGA + U), we find the means for both sets to be close to zero (−1.1 ± 21 meV/atom in GGA and −4.6 ± 6.3 meV/atom for GGA + U) showing no conclusive difference in terms of the mean and therefore in the tendency to overestimate or underestimate reaction energies. On the other hand, the standard deviation is significantly higher for GGA (69 ± 15 meV/atom) than for GGA + U (19 ± 5.3 meV/atom), indicating significantly larger errors when no Hubbard U

TABLE III. Difference between computed and experimental reaction energies in GGA + U for reaction energies involving change in formal oxidation states (as defined by the ICSD).

Reaction	Change in oxidation state	$\Delta E^{\mathrm{comp}}_{\mathrm{GGA}+U} - \Delta E^{\mathrm{expt}}_{0\,\mathrm{K}}$ (meV/atom)
$\frac{2}{3}\mathrm{Fe_3O_4} + \frac{1}{3}\mathrm{Mn_3O_4} \rightarrow \mathrm{Fe_2MnO_4}$	$\mathrm{Fe^{2+}, Mn^{3+} \rightarrow Fe^{3+}, Mn^{2+}}$	14
$\frac{1}{2}\mathrm{Fe_2O_3} + \frac{1}{2}\mathrm{MoO_3} + \frac{1}{2}\mathrm{MoO_2} \rightarrow \mathrm{FeMoO_4}$	$\mathrm{Fe^{3+}, Mo^{4+} \rightarrow Fe^{2+}, Mo^{6+}}$	14
$\frac{1}{2}\mathrm{Mn_2O_3} + \frac{1}{2}\mathrm{MoO_3} + \frac{1}{2}\mathrm{MoO_2} \rightarrow \mathrm{MnMoO_4}$	$\mathrm{Mn^{3+}, Mo^{4+} \rightarrow Mn^{2+}, Mo^{6+}}$	34

parameter is used. Table IV illustrates this result by presenting the compounds with the largest difference between the error with GGA + U and the error with GGA. Some reactions, such as those forming $\mathrm{FeMoO_4}$ and $\mathrm{Fe_2MnO_4}$, involve change in formal oxidation states and are, not surprisingly, better represented with GGA + U. However, even reaction energies without any change in formal valence (i.e., the reactions forming $\mathrm{NaFeO_2}$, $\mathrm{Cr_2FeO_4}$, $\mathrm{Co_2SiO_4}$, $\mathrm{MnTiO_3}$, and $\mathrm{Mn_2TiO_4}$) show better accuracy in GGA + U. This is likely due to the fact that all reactions, even those without a formal change in oxidation state, can involve change in bonding and charge transfer. The use of the Hubbard U is therefore necessary to correct for the self-interaction error arising from these charge transfers.

In contrast to most previous work comparing experimental thermochemical data with DFT results, we performed a heat-capacity integration to make sure we compare DFT results to 0 K energies (instead of 298 K). When formation energies are calculated from the elements, the DFT error (rms of 200 meV/atom)[52] is so large that the heat-capacity integration is not relevant. However, in our study where the DFT error is smaller, it is difficult to *a priori* decide to neglect the heat-capacity integration down to 0 K. Comparing the error distribution obtained with and without the heat-capacity integration, we observe a larger standard deviation when the integrated heat capacity is not taken into account (31 ± 4.2 meV/atom versus 24 ± 3.5 meV/atom). On average, the contribution of the heat-capacity integration is smaller than the DFT error (mean absolute component of the heat-capacity integration is 12 meV/atom), but for some reactions, its effect can be large enough to be necessary to achieve a good accuracy. We present in Table V a few of the reaction energies with the largest integrated heat-capacity components (i.e., the largest $|\Delta E^{\mathrm{expt}}_{298\,\mathrm{K}} - \Delta E^{\mathrm{expt}}_{0\,\mathrm{K}}|$). For all those reactions, including the heat-capacity component improves the agreement between computations and experiments. Many of those reactions involve aluminum-based compounds because of a large mismatch between the Debye temperature for $\mathrm{Al_2O_3}$ (897 K) and for some of the aluminum-containing ternaries such as $\mathrm{Ba_3Al_2O_6}$ (308 K), $\mathrm{Ca_3Al_2O_6}$ (523 K), and $\mathrm{CaAl_4O_7}$ (593 K).

IV. DISCUSSION

We have presented a comparison between experimental and DFT energies of reactions across a large set of oxide chemistries and crystal structures. For a data set of reaction energies relevant to phase stability, the distribution of the error between GGA + U computations and experiments has been provided. In addition, we analyzed how those errors depend on chemistries and are influenced by the use of a Hubbard U parameter.

While we tried as much as possible to remove unreliable experimental data from our data set, we must stress that our results depend on the quality of the experimental data. Our work already identified a few large discrepancies between the Kubachewski tables and data from NIST (e.g., $\mathrm{K_2SiO_3}$ with a 216-meV/atom difference, and $\mathrm{Mg_2Ti_2O_5}$ with a 72-meV/atom difference), or the Landolt-Bornstein database ($\mathrm{FeMoO_4}$ with a 20-meV/atom discrepancy, $\mathrm{Na_4V_2O_7}$ with a 88-meV/atom discrepancy, $\mathrm{Na_2MoO_4}$with a 97-meV/atom discrepancy, and $\mathrm{KFeO_2}$ with a 1420-meV/atom error), as well as very likely errors in both of these databases (e.g., $\mathrm{Na_2Mo_2O_7}$ and $\mathrm{BaMoO_4}$). Another possible source of error in our data set can come from an inadequate choice of crystal structure among polymorphs as only partial crystallographic information is usually provided in the Kubachewski tables (e.g., $\mathrm{Ca_3(PO_4)_2}$).

A few computational assumptions also influence our results. Due to the high-throughput nature of our investigation, we only tested specific magnetic states of compounds: FM or AFM. Any magnetic ground state more complex would have been missed. In addition, the U value we used has been fitted

TABLE IV. Difference between computed and reaction energies for GGA + U and GGA. Only the reactions with the largest difference between GGA and GGA + U results are presented (>50 meV/atom).

Reaction	$\Delta E^{\mathrm{comp}}_{\mathrm{GGA}} - \Delta E^{\mathrm{expt}}_{0\,\mathrm{K}}$ (meV/atom)	$\Delta E^{\mathrm{comp}}_{\mathrm{GGA}+U} - \Delta E^{\mathrm{expt}}_{0\,\mathrm{K}}$ (meV/atom)
$\frac{2}{3}\mathrm{Fe_3O_4} + \frac{1}{3}\mathrm{Mn_3O_4} \rightarrow \mathrm{Fe_2MnO_4}$	355	14
$\mathrm{Cr_2O_3 + FeO \rightarrow Cr_2FeO_4}$	71	−14
$\mathrm{2CoO + SiO_2 \rightarrow Co_2SiO_4}$	64	−12
$\mathrm{MnO + TiO_2 \rightarrow MnTiO_3}$	−76	−25
$\mathrm{2MnO + TiO_2 \rightarrow Mn_2TiO_4}$	−88	−10
$\frac{1}{2}\mathrm{Fe_2O_3} + \frac{1}{2}\mathrm{MoO_3} + \frac{1}{2}\mathrm{MoO_2} \rightarrow \mathrm{FeMoO_4}$	−74	14
$\frac{1}{2}\mathrm{Na_2O} + \frac{1}{2}\mathrm{Fe_2O_3} \rightarrow \mathrm{NaFeO_2}$	−128	−51

TABLE V. Comparison between experimental 0-K energy (with heat-capacity integration) and experimental 298-K energy for the compounds with the largest influence of the heat-capacity integration on the reaction energy (>40 meV/atom).

Reaction	$\Delta E^{\text{expt}}_{298\,\text{K}} - \Delta E^{\text{expt}}_{0\,\text{K}}$ (meV/atom)	$\Delta E^{\text{comp}}_{0\,\text{K}} - \Delta E^{\text{expt}}_{0\,\text{K}}$ (meV/atom)	$\Delta E^{\text{comp}}_{0\,\text{K}} - \Delta E^{\text{expt}}_{298\,\text{K}}$ (meV/atom)
$2Na_2O + V_2O_5 \rightarrow Na_4V_2O_7$	47	3	−45
$K_2O + 2B_2O_3 \rightarrow K_2B_4O_7$	−45	0	45
$Al_2O_3 + 3BaO \rightarrow Ba_3Al_2O_6$	42	17	−25
$Al_2O_3 + 3CaO \rightarrow Ca_3Al_2O_6$	54	−21	−75
$2Al_2O_3 + 3CaO \rightarrow CaAl_4O_7$	52	−42	−93

on binary oxide formation enthalpies and directly influences the energies obtained. Finally, our results rely on the PAW pseudopotentials used, and would be influenced by any error in their construction or transferability.[66]

The available experimental thermochemical data present some chemical biases influencing our results. While our data cover main group and transition metals well, the rare-earth and actinides are not as well sampled due to the lack of experimental data available. Future work on those chemistries, relying mainly on extracting more experimental data, would be required to more precisely evaluate the accuracy of their reaction energies. The most straightforward use of our result is in error detection. By combining DFT computations with our error distribution, we can test the accuracy of uncertain experimental data. For instance, during our experimental data cross-checking process (see Sec. II), we identified seven compounds ($NaVO_3$, SrB_4O_7, $LiTaO_3$, $LiNbO_3$, $LaPO_4$, LiB_3O_5, and $CdTiO_3$) for which the enthalpy provided by the Kubachewski database could not be confirmed by other reliable sources and that we had to exclude from our data set. Among those seven compounds, we find three compounds, the computed formation reaction energies of which differ from the reported experimental value by a large enough extent to cast major doubt on the Kubachewski data ($NaVO_3$ by 87 meV/atom, $CdTiO_3$ by 89 meV/atom, and $LiNbO_3$ by 106 meV/atom).

Another critical application of our results lies in the assessment of the accuracy of 0-K phase diagrams built from GGA + U computations. These phase diagrams are useful when studying the phase stability of known but also predicted compounds. Several recent studies relied on such phase diagrams to investigate the stability of new proposed phosphates-based compounds for lithium-ion batteries,[20–22] new predicted ternary oxides,[18] new iron borides,[17] or new intermetallics.[16,26] 0-K phase diagrams based on GGA computations for all compounds in the ICSD are also available online through the *Materials Project*.[40,67] 0-K phase diagrams are typically built using the convex-hull construction, which effectively evaluates the stability for a given compound against any linear combination of compounds that has the same composition. From this construction, there is one critical reaction energy that will ultimately determine if a compound is stable (on the convex hull) or not (see Sec. II). It is very common for those critical reactions to involve only very chemically similar compounds when multicomponent systems are studied. For instance, we show in Fig. 5(a) the Li-Al-O phase diagram constructed from the calculated energy of the relevant phases in the ICSD. The black arrows indicate which phases will be involved in the reaction critical to phase stability. For the two ternary oxides $LiAlO_2$ and Li_5AlO_4, the reaction energies determining their stability are, respectively, $\frac{1}{5}Li_5AlO_4 + \frac{2}{5}Al_2O_3 \rightarrow LiAlO_2$ and $2Li_2O + LiAlO_2 \rightarrow Li_5AlO_4$. The relevant reaction energies involve oxides (i.e., chemically similar compounds) and, while there are metallic elements (Li and Al) and intermetallics ($LiAl$, Li_3Al, Li_3Al_2) present in the phase diagram, those are not directly involved in determining whether the ternary oxides are stable or not. Figure 5(b) shows the Li-Cr-O phase diagram which is more complicated due to the large number of oxidation states that Cr can form (+3 to +6). For $LiCrO_2$, the reaction determining phase stability is $\frac{1}{2}Cr_2O_3 + \frac{1}{2}Li_2O \rightarrow LiCrO_2$. Again, this reaction involves only Cr^{3+}-based oxides. The reaction energies with respect to the elements or chromium phases at other oxidation states (e.g., CrO_2, CrO_3, and Li_2CrO_4) do not directly influence the stability of $LiCrO_2$. Similarly, the stability of Li_2CrO_4 depends directly on reaction energies with respect with Li_2O and another Cr^{6+} oxide: CrO_3. On the other hand, Li_3CrO_4 depends on a more complicated reaction involving Li_2CrO_4, $LiCrO_2$, and Li_2O. This reaction still does not involve metallic elemental phases but is a redox reaction (involving Cr in +3 and +6 states).

The situation we illustrated with the Li-Al-O and Li-Cr-O phase diagrams is very common. For all ternary oxides present in the ICSD database, 80% compete for phase stability through reactions involving only oxide reactions with no change in formal oxidation state. In those common cases, the DFT error distribution we found in our work can be used to assess the accuracy of 0-K GGA + U phase diagrams. For instance, when a new compound is proposed, its energy for decomposition to other stable phases can be computed through the convex-hull constructions. Using the DFT error distribution, we can take into account inherent errors within DFT and evaluate the likelihood for a DFT error to result in incorrectly predicting the stability of a compound. For example, a compound computed to be 50 meV/atom above the convex hull (i.e., having a decomposition energy to other phases around 50 meV/atom) is likely to actually be unstable at 0 K as such a large error would be two standard deviations away from the mean. Similarly, when a predicted compound is stable versus competing phases (i.e., on the convex hull), our error distribution can be used to assess the probability that its stability is due to a DFT error. We should note that, while not common, there are instances

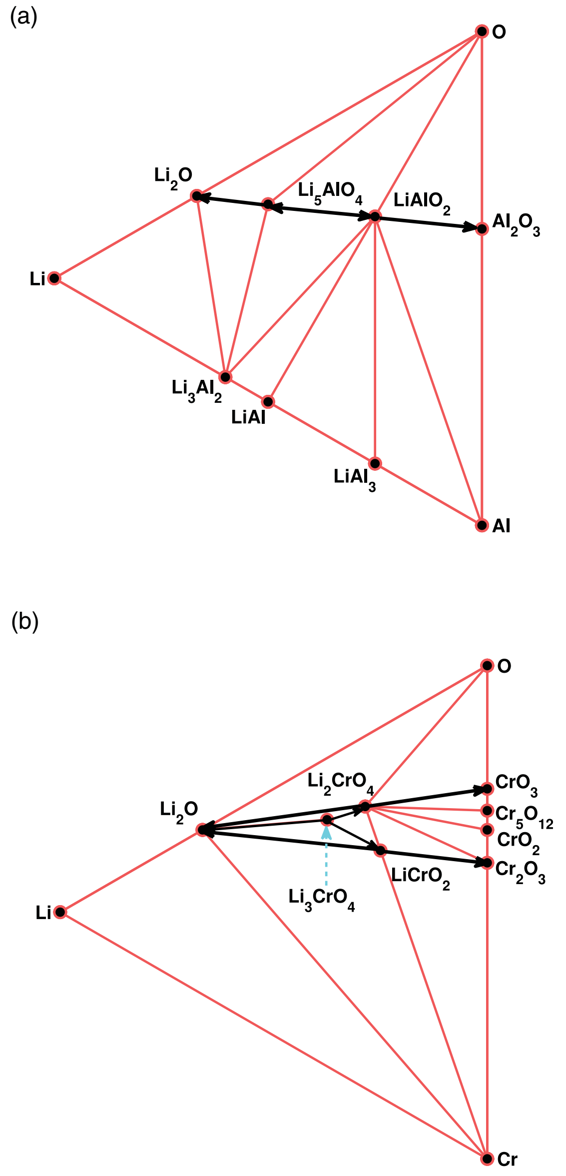

FIG. 5. (Color online) Two examples of ternary oxides 0-K phase diagrams: Li-Al-O (a) and Li-Cr-O (b). All phases are from the ICSD. We excluded phases with partial occupancies. The Li-Al-O phase diagram illustrates the case of elements with only one oxidation state. On the other hand, Cr in the Li-Cr-O phase diagram is common in oxidation states from +3 to +6. The black (dark gray) arrows indicate the critical reaction energies determining the stability of ternary phases. The light blue (gray) dashed arrow indicates the Li_3CrO_4 phase.

where the reaction energy critical to phase stability involves compounds very different chemically (e.g., a ternary oxide competing versus a metal or versus phases with different oxidation states). In those cases, caution must be exerted in the interpretation of the results, and it is possible that the typical errors can be larger than those presented in this work. While our study did not show any large discrepancy for reaction energies involving oxides with different oxidation states, our data set (three reactions) was too limited to derive strong conclusions. On the other hand, it is extremely likely that the errors on reaction energies involving oxides and metallic phases will be much higher than the errors obtained in this work. Indeed, solid elemental phases are often metallic and formation energies from the elements for ternary oxides show much larger errors due to smaller cancellation of errors.[51,52,68]

By noting that most reactions relevant for phase stability involve chemically similar compounds and providing an error distribution for those reactions, our work also removes an apparent paradox on the accuracy of 0-K phase diagram. DFT-calculated 0-K phase diagrams are often quite accurate in predicting the correct stable phases. The Li-Fe-P-O phase diagram presented in Ong *et al.*[10] for instance shows very good agreement with experimental phase stability. This success is surprising when compared with the magnitude of the reported errors in DFT elemental formation energies (rms of 240 meV/atom).[52] Our work resolves this apparent contradiction by noting that reaction energies from the elements are in general not relevant to phase stability and that the error distribution is much smaller for the reaction energies relevant to phase stability.

Interestingly, our work shows that, when transition metals with partially occupied d shell are involved, the accuracy of DFT is significantly lower for GGA than for GGA + U, even for reaction energies involving no change in formal oxidation state. Unfortunately, GGA + U is known to fail at modeling metallic and intermetallic phases, leading to larger errors in the regions of the phase diagram involving those phases. Our results reinforce the need to use either higher-level theories or schemes to mix GGA and GGA + U such as the one developed by Jain *et al.*[68] to obtain accurate phase diagrams that cover chemically diverse regions of composition space.

This work only focused on oxides due to the lack of thermochemical data in other types of ternary semiconducting or insulating materials (e.g., halides or sulfides). However, we believe that the conclusions might be of more general character. The very limited set of fluorides present in the Kubachewski tables (Li_2BeF_4, Li_3AlF_6, and Na_3AlF_6) show errors for reaction energies from binary to ternary fluorides of, respectively, −20 meV/atom, −6 meV/atom, and 6 meV/atom, which are within the error distribution found for oxides. We should, however, warn the reader that our data did not include any peroxides (i.e., oxides containing oxygen-oxygen bonds as O_2^{2-}) and we have experienced that peroxides tend to be overstabilized in GGA due to the overbinding of the O-O bond (similarly to the overbinding of the oxygen molecule).[69] While peroxides are rare, other chemistries such as sulfides or nitrides tend to form those types of covalent bonds more easily in solids (e.g., persulfides or pernitrides) and might suffer more often from this possible error.

We hope the work presented in this paper will motivate future thermochemical evaluation of alternative functionals. It would be for instance of interest to compare the performances of new functionals, such as AM05 and HSE,[70–73] or more advanced techniques, such as quantum Monte Carlo,[74] to GGA + U. While bulk modulus and lattice constants are often tested when new methods or functionals are proposed, it is rare to evaluate the accuracy of reaction energies. We hope the material provided in this work can constitute a standard data set to perform future benchmarks.

V. CONCLUSION

We have estimated the error in GGA $+ U$ in reproducing reaction energies relevant to phase stability in ternary oxides. This error is distributed normally with a mean close to zero and a standard deviation of 24 meV/atom. The errors we found are much smaller than the error on the more commonly reported reaction energies from the elements. We attribute this to the larger cancellation of errors involved in reaction energies among chemically similar compounds. Our results can be used to assess the accuracy of 0-K phase diagrams as the relevant reaction energies when building phase diagrams involve chemically similar compounds. Finally, our analysis also demonstrates the importance of using a Hubbard U parameter to model reaction energies involving transition metals even when no change in formal oxidation states is occurring.

ACKNOWLEDGMENTS

The authors would like to acknowledge C. Fischer and T. Mueller for helpful discussion. This work was supported by the NSF (under Contract No. DMR-0606276) and by the Department of Energy, Office of Basic Energy Sciences (under Contract No DE-FG02-96ER4557). A. Jain would like to acknowledge funding from the US Department of Energy through the Department of Energy Computational Science Graduate Fellowship (DOE CSGF) (under Grant No. DE-FG02-97ER25308).

APPENDIX A

Table VI gives the VASP pseudopotentials used in this work and the value of the Hubbard U (if any) on each element.

TABLE VI. VASP PAW pseudopotentials and U parameters (if any) used for each element.

Element	VASP PAW pseudopotential	U (eV)	Element	VASP PAW pseudopotential	U (eV)
Ag	Ag 06Sep2000	1.5	Li	Li 17Jan2003	
Al	Al 04Jan2001		Mg	Mg 05Jan2001	
Ba	Ba_sv 06Sep2000		Mn	Mn 06Sep2000	3.9
B	B 06Sep2000		Mo	Mo_pv 08Apr2002	4.38
Be	Be 06Sep2000		Na	Na 08Apr2002	
Ca	Ca_sv 06Sep2000		Nb	Nb_pv 08Apr2002	1.5
Cd	Cd 06Sep2000		Ni	Ni 06Sep2000	6.0
Ce	Ce 28Sep2000		O	O 08Apr2002	
Co	Co 06Sep2000	3.4	Pb	Pb 08Apr2002	
Cr	Cr 06Sep2000	3.5	P	P 17Jan2003	
Cs	Cs_sv 08Apr2002		Rb	Rb_pv 06Sep2000	
Cu	Cu 05Jan2001	4.0	Se	Se 06Sep2000	
Fe	Fe 06Sep2000	4.0	Si	Si 05Jan2001	
Ge	Ge 05Jan2001		Sr	Sr$_{sv}$ 07Sep2000	
Hf	Hf 20Jan2003		Ti	Ti 08Apr2002	
Hg	Hg 06Sep2000		U	U 06Sep2000	
K	K_sv 06Sep2000		V	V_pv 07Sep2000	3.1
La	La 06Sep2000		Zn	Zn 06Sep2000	
			Zr	Zr 08Apr2002	

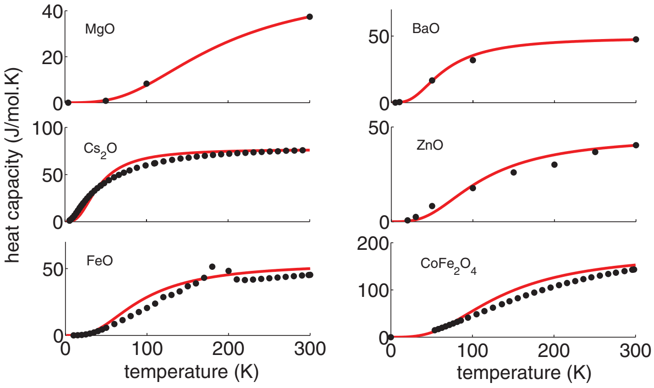

FIG. 6. (Color online) Heat capacity vs temperature for several compounds (MgO, BaO, ZnO, Cs_2O, FeO, and $CoFe_2O_4$). The black dots are experimental values and the red line is the fitted Debye-type model. All heat capacities are given in J/mol-fu K.

APPENDIX B

Heat-capacity data down to 0 K is not available for all compounds used in our work. To obtain the enthalpy at 0 K from the provided enthalpies at 298 K, we estimated the heat capacity at low temperature by a fitting procedure (see Sec. II). We used the experimental heat capacity and entropy at 298 K to fit a Debye-type model. This model was then integrated down to 0 K and substracted from the enthalpy at 298 K to provide the enthalpy at 0 K. In this section, we will compare, for a few compounds which have experimentally known heat-capacity data, the results of our fitting procedure to the direct heat-capacity measurement.

Figure 6 shows the heat capacity versus temperature curve fitted to the Debye-type model (red line) and experimentally determined for a few compounds: MgO,[75] BaO,[75] ZnO,[75] Cs_2O,[76] FeO,[77] and $CoFe_2O_4$.[47] A very good agreement between both data sets can be observed for all compounds, validating our approach.

Table VII shows the difference between the integrated heat capacity from 0 to 298 K from our fitted model and obtained directly from experiments. The good agreement in terms of heat capacity versus temperature curves is reflected into the small difference between the integrated heat capacity (from 2 to 5 meV/atom).

Our approach was not aimed at reproducing very accurately the Debye temperature, but we compared our fitted

TABLE VII. Integrated heat capacity from 0 to 298 K. Values obtained directly from experiments and through the fitted Debye model.

Formula	Integrated heat capacity from direct experiment (meV/atom)	Integrated heat capacity from fitted Debye model (meV/atom)	Difference (meV/atom)
MgO	24.9	26.6	1.7
BaO	49.2	53.6	4.4
Cs_2O	61.9	63.9	2.0
ZnO	35.6	37.7	2.1
FeO	45.4	50.1	4.7
$CoFe_2O_4$	32.6	37.2	4.6

Debye temperature to noncalorimetric-based Debye temperature measurements when present in the Landolt-Bornstein database. From neutron scattering experiments on MgO, the Debye temperature is reported to be 743 K and our fitted value is 779 K. From elastic constant measurements, we find 291 K for BaO, 416 K for ZnO, and 494 K for FeO, which compares well with 266, 455, and 383 K, respectively, found from our fit.

APPENDIX C

Table VIII gives the ICSD number of the corresponding crystal structure, the experimental formation energy from the element (given at 0 K through heat-capacity integration), the experimental error on the formation enthalpy from the element, the computed total energy (in GGA and GGA + U), and the source of the experimental data.

TABLE VIII. ICSD reference number, experimental formation enthalpy, experimental error, computed total energy with GGA + U, and GGA and the source (Kubachewski or NIST) for each compound. The experimental formation enthalpies are given at 0 K through heat capacity integration.

Formula	ICSD number	Expt. formation enthalpy (eV/atom)	Expt. error (eV/atom)	Computed total energy GGA + U (eV/atom)	Computed total energy GGA (eV/atom)	Source
Ag_2CrO_4	16298	−1.114	0.011	−5.265	−6.045	Kuba
Ag_2O	35540	−0.162	0.002	−3.195	−3.63	Kuba
$AlCeO_3$	72558	−3.767	0.006	−8.08	−8.08	Kuba
$AlLaO_3$	92523	−3.75	0.007	−8.015	−8.015	Kuba
$AlLiO_2$	28288	−3.106	0.011	−6.614	−6.614	Kuba
$AlNaO_2$	79404	−2.968	0.011	−6.351	−6.351	NIST
$AlPO_4$	72374	−3.021	0.004	−7.476	−7.476	Kuba
Al_2BaO_4	75426	−3.475	0.012	−7.226	−7.226	Kuba
$Al_2Ba_3O_6$	79558	−3.348	0.012	−6.79	−6.79	Kuba
Al_2BeO_4	31080	−3.427	0.009	−7.394	−7.394	Kuba
Al_2CaO_4	260	−3.473	0.003	−7.245	−7.245	Kuba
$Al_2Ca_3O_6$	1841	−3.416	0.004	−6.947	−6.947	Kuba
Al_2FeO_4	56117	−2.94	0.004	−7.34	−7.504	Kuba
Al_2MgO_4	29444	−3.431	0.011	−7.11	−7.11	NIST
Al_2O_3	43732	−3.494	0.003	−7.481	−7.481	Kuba
Al_2SrO_4	26466	−3.492	0.025	−7.205	−7.205	Kuba
Al_2ZnO_4	94158	−3.091	0.004	−6.706	−6.706	Kuba
Al_2SiO_5	28272	−3.384	0.011	−7.633	−7.633	NIST
Al_2TiO_5	24133	−3.404	0.022	−7.976	−7.976	Kuba
Al_4CaO_7	34487	−3.481	0.003	−7.364	−7.364	Kuba
Al_6BeO_{10}	95408	−3.45	0.006	−7.444	−7.444	Kuba
$BCsO_2$	74888	−2.57	0.054	−6.626	−6.626	Kuba
BKO_2	16005	−2.611	0.022	−6.725	−6.725	Kuba
$BLiO_2$	16568	−2.665	0.004	−7.017	−7.017	Kuba
$BNaO_2$	34645	−2.559	0.006	−6.759	−6.759	Kuba
$BRbO_2$	59826	−2.564	0.054	−6.649	−6.649	Kuba
B_2CaO_4	20097	−3.028	0.006	−7.756	−7.756	Kuba
$B_2Ca_2O_5$	280076	−3.165	0.006	−7.532	−7.532	Kuba
$B_2Ca_3O_6$	23664	−3.257	0.004	−7.372	−7.372	Kuba
B_2O_3	24047	−2.66	0.004	−8.023	−8.023	Kuba
B_3NaO_5	2045	−2.671	0.008	−7.532	−7.532	Kuba
B_4CaO_7	200081	−2.907	0.005	−7.902	−7.902	Kuba
$B_4K_2O_7$	2833	−2.683	0.011	−7.292	−7.292	NIST
$B_4Li_2O_7$	300010	−2.704	0.011	−7.445	−7.445	NIST
$B_4Na_2O_7$	2040	−2.638	0.011	−7.304	−7.304	NIST
$B_8Na_2O_{13}$	14355	−2.682	0.005	−7.654	−7.654	Kuba
$BaMoO_4$	50821	−2.659	0.012	−7.088	−7.954	Kuba
BaO	52278	−2.894	0.011	−5.913	−5.913	Kuba
$BaSiO_3$	6245	−3.389	0.015	−7.405	−7.405	Kuba
$BaTiO_3$	31155	−3.453	0.024	−7.935	−7.935	Kuba
$BaZrO_3$	97462	−3.709	0.012	−8.296	−8.296	Kuba
$BaUO_4$	36239	−3.483	0.004	−8.705	−8.705	Kuba
Ba_2SiO_4	6246	−3.405	0.006	−7.119	−7.119	Kuba
Ba_2TiO_4	2625	−3.351	0.019	−7.45	−7.45	Kuba
BeO	29271	−3.173	0.017	−7.11	−7.11	Kuba
Be_2SiO_4	85484	−3.155	0.011	−7.459	−7.459	NIST

TABLE VIII. *(Continued.)*

Formula	ICSD number	Expt. formation enthalpy (eV/atom)	Expt. error (eV/atom)	Computed total energy GGA + U (eV/atom)	Computed total energy GGA (eV/atom)	Source
$CaCr_2O_4$	6131	−2.743	0.011	−7.542	−8.144	Kuba
$CaFe_2O_4$	28177	−2.228	0.011	−6.756	−7.247	Kuba
$CaGeO_3$	403086	−2.697	0.011	−6.558	−6.558	Kuba
$CaMoO_4$	409785	−2.706	0.006	−7.087	−7.951	Kuba
$CaNb_2O_6$	15208	−3.116	0.02	−8.223	−8.551	Kuba
CaO	52783	−3.325	0.004	−6.439	−6.439	Kuba
$CaSiO_3$	201538	−3.419	0.004	−7.49	−7.49	Kuba
$CaTiO_3$	94568	−3.476	0.01	−8.016	−8.016	Kuba
$CaZrO_3$	37264	−3.696	0.02	−8.345	−8.345	Kuba
$CaUO_4$	31631	−3.488	0.007	−8.747	−8.747	Kuba
CaV_2O_6	21064	−2.717	0.006	−7.43	−8.14	Kuba
$Ca_2Fe_2O_5$	88989	−2.495	0.006	−6.686	−7.143	Kuba
Ca_2SiO_4	9095	−3.479	0.008	−7.259	−7.259	Kuba
$Ca_2P_2O_7$	22225	−3.174	0.02	−7.27	−7.27	Kuba
$Ca_2V_2O_7$	20609	−2.94	0.006	−7.352	−7.942	Kuba
$Ca_3Si_2O_7$	34354	−3.437	0.011	−7.352	−7.352	Kuba
$Ca_3P_2O_8$	200202	−3.314	0.02	−7.243	−7.243	Kuba
$Ca_3V_2O_8$	412273	−3.048	0.007	−7.218	−7.73	Kuba
$Ca_4Ti_3O_{10}$	86242	−3.493	0.011	−7.828	−7.828	Kuba
CdO	24802	−1.384	0.004	−3.956	−3.956	Kuba
$CdSeO_3$	75274	−1.237	0.011	−4.851	−4.851	Kuba
$CeCrO_3$	4115	−3.216	0.024	−8.329	−8.643	Kuba
Ce_2O_3	96202	−3.778	0.003	−8.687	−8.687	Kuba
$CoCr_2O_4$	61612	−2.155	0.01	−7.436	−8.194	Kuba
CoO	17013	−1.279	0.003	−5.62	−6.656	Kuba
$CoSeO_3$	80401	−1.238	0.022	−5.636	−5.824	Kuba
$CoTiO_3$	48107	−2.539	0.008	−7.756	−7.976	Kuba
Co_2SiO_4	65751	−2.109	0.007	−6.856	−7.145	Kuba
$CrCs_2O_4$	30204	−2.164	0.005	−5.828	−6.443	Kuba
CrK_2O_4	2402	−2.103	0.006	−5.887	−6.495	Kuba
$CrNaO_2$	24595	−2.308	0.012	−6.606	−7.101	Kuba
$CrNa_2O_4$	26330	−2.017	0.014	−5.892	−6.503	Kuba
CrO_3	38125	−1.554	0.028	−6.565	−7.624	Kuba
Cr_2CuO_4	16708	−1.95	0.011	−6.864	−7.679	Kuba
Cr_2FeO_4	43269	−2.178	0.007	−7.657	−8.383	Kuba
Cr_2MgO_4	97202	−2.661	0.005	−7.415	−7.993	Kuba
Cr_2NiO_4	28835	−2.071	0.006	−6.879	−7.938	Kuba
Cr_2O_3	107035	−2.384	0.016	−7.888	−8.739	Kuba
Cr_2ZnO_4	24495	−2.324	0.007	−7.012	−7.575	Kuba
Cs_2MoO_4	9278	−2.293	0.011	−5.94	−6.697	Kuba
Cs_2O	27919	−1.259	0.01	−3.2	−3.2	Kuba
Cs_2UO_4	20581	−2.905	0.007	−7.321	−7.321	Kuba
CuO	67850	−0.846	0.011	−4.272	−4.917	NIST
$FeKO_2$	94467	−1.83	0.011	−5.794	−6.21	Kuba
$FeMoO_4$	43013	−1.889	0.011	−7.069	−8.136	Lando
$FeNaO_2$	33763	−1.848	0.015	−5.882	−6.444	Kuba
FeO	76639	−1.46	0.036	−6.515	−7.539	Kuba
$FeTiO_3$	9805	−2.602	0.012	−8.073	−8.363	Kuba
Fe_2MnO_4	24497	−1.858	0.007	−7.126	−7.545	Kuba
Fe_2O_3	41541	−1.74	0.007	−6.781	−7.511	Kuba
Fe_2SiO_4	34817	−2.214	0.012	−7.36	−7.66	Kuba
Fe_2ZnO_4	91827	−1.779	0.009	−6.221	−6.618	Kuba
Fe_3O_4	31157	−1.697	0.011	−6.805	−7.633	NIST
$GeMgO_3$	35534	−2.532	0.01	−6.291	−6.291	Kuba
GeO_2	92551	−2.029	0.005	−6.39	−6.39	Kuba
HfO_2	27313	−3.896	0.006	−10.189	−10.189	Kuba
$HfSrO_3$	86830	−3.736	0.025	−8.704	−8.704	Kuba

TABLE VIII. *(Continued.)*

Formula	ICSD number	Expt. formation enthalpy (eV/atom)	Expt. error (eV/atom)	Computed total energy GGA + U (eV/atom)	Computed total energy GGA (eV/atom)	Source
HgO	14124	−0.522	0.004	−2.914	−2.914	Kuba
$HgSeO_3$	412547	−0.804	0.011	−4.357	−4.357	Kuba
K_2O	60438	−1.311	0.01	−3.409	−3.409	Kuba
K_2SiO_3	201163	−2.712	0.011	−6.078	−6.078	NIST
$K_2Si_2O_5$	52156	−2.924	0.01	−6.723	−6.723	Kuba
$K_2Si_4O_9$	2155	−3.015	0.01	−7.217	−7.217	Kuba
La_2O_3	96201	−3.763	0.006	−8.405	−8.405	Kuba
$LiPO_3$	85714	−2.628	0.008	−6.725	−6.725	Kuba
Li_2O	57411	−2.091	0.003	−4.771	−4.771	Kuba
Li_2SiO_3	16626	−2.873	0.018	−6.563	−6.563	Kuba
Li_2TiO_3	15150	−2.913	0.018	−7.008	−7.008	Kuba
Li_2ZrO_3	31941	−3.073	0.012	−7.243	−7.243	Kuba
$MgMoO_4$	20418	−2.453	0.009	−6.79	−7.658	Kuba
MgO	52026	−3.144	0.002	−5.983	−5.983	Kuba
$MgSiO_3$	30893	−3.236	0.008	−7.189	−7.189	Kuba
$MgTiO_3$	55285	−3.288	0.004	−7.743	−7.743	Kuba
$MgUO_4$	24725	−3.243	0.005	−8.443	−8.443	Kuba
$MgTi_2O_5$	37232	−3.283	0.011	−8.159	−8.159	NIST
MgV_2O_6	10391	−2.566	0.006	−7.21	−7.921	Kuba
Mg_2SiO_4	88023	−3.249	0.004	−6.885	−6.885	Kuba
$Mg_2V_2O_7$	93603	−2.703	0.008	−7.048	−7.645	Kuba
$Mg_3P_2O_8$	31005	−3.014	0.011	−6.886	−6.886	NIST
$MnMoO_4$	15615	−2.097	0.017	−7.409	−8.444	Kuba
MnO	53928	−2.042	0.007	−7.764	−8.238	Kuba
$MnSiO_3$	34160	−2.772	0.005	−7.903	−8.087	Kuba
$MnTiO_3$	60006	−2.854	0.011	−8.481	−8.715	Kuba
Mn_2O_3	9090	−2.025	0.004	−7.501	−8.235	Kuba
Mn_2SiO_4	26376	−2.601	0.006	−7.904	−8.176	Kuba
Mn_2TiO_4	22313	−2.632	0.011	−8.283	−8.622	Kuba
Mn_3O_4	76088	−2.092	0.003	−7.627	−8.345	Kuba
$MoNa_2O_4$	44523	−2.214	0.011	−6.082	−6.825	Lando
MoO_2	36263	−2.06	0.006	−7.618	−8.802	Kuba
MoO_3	76365	−1.965	0.002	−6.99	−8.256	Kuba
$MoPbO_4$	39137	−1.862	0.009	−6.623	−7.481	Kuba
$MoSrO_4$	23700	−2.713	0.017	−7.061	−7.925	Kuba
$Mo_2Na_2O_7$	24312	−2.263	0.012	−6.461	−7.392	Kuba
$NaPO_3$	18139	−2.562	0.004	−6.556	−6.556	Kuba
Na_2O	60435	−1.486	0.011	−3.781	−3.781	NIST
Na_2SiO_3	24664	−2.734	0.011	−6.201	−6.201	Kuba
Na_2UO_4	79423	−2.838	0.004	−7.47	−7.47	Kuba
$Na_2Si_2O_5$	34688	−2.88	0.006	−6.785	−6.785	Kuba
$Na_2Ti_3O_7$	15463	−3.042	0.004	−7.749	−7.749	Kuba
Na_3PO_4	97205	−2.52	0.003	−5.851	−5.851	Kuba
Na_4SiO_4	15500	−2.458	0.029	−5.509	−5.509	Kuba
$Na_4P_2O_7$	10370	−2.56	0.011	−6.165	−6.165	Kuba
$Na_4V_2O_7$	35635	−2.374	0.011	−6.204	−6.708	Lando
Nb_2O_5	25750	−2.847	0.006	−8.583	−8.96	Kuba
NiO	24018	−1.278	0.007	−5.059	−5.748	Kuba
$NiSeO_3$	416251	−1.212	0.011	−5.221	−5.493	Kuba
$NiTiO_3$	15988	−2.523	0.013	−7.349	−7.654	Kuba
Ni_2SiO_4	202376	−2.103	0.014	−6.313	−6.714	Kuba
PbO	94333	−1.187	0.004	−5.426	−5.426	Kuba
Rb_2O	77676	−1.23	0.029	−3.159	−3.159	Kuba
SrO	28904	−3.113	0.02	−6.052	−6.052	Kuba
ZnO	31060	−1.854	0.003	−4.549	−4.549	Kuba
SeO_2	24022	−0.815	0.007	−5.151	−5.151	Kuba
SiO_2	98629	−3.172	0.006	−7.904	−7.904	Kuba
TiO_2	69331	−3.292	0.003	−8.804	−8.804	Kuba

TABLE VIII. *(Continued.)*

Formula	ICSD number	Expt. formation enthalpy (eV/atom)	Expt. error (eV/atom)	Computed total energy GGA + U (eV/atom)	Computed total energy GGA (eV/atom)	Source
ZrO_2	68782	−3.823	0.011	−9.517	−9.517	NIST
$PbSeO_3$	1271	−1.159	0.011	−5.438	−5.438	Kuba
$PbSiO_3$	26812	−2.408	0.011	−6.968	−6.968	NIST
$PbTiO_3$	27949	−2.515	0.029	−7.488	−7.488	Kuba
$SeZnO_3$	61341	−1.387	0.008	−5.003	−5.003	Kuba
$SiSrO_3$	38271	−3.419	0.008	−7.42	−7.42	Kuba
$SrTiO_3$	56718	−3.5	0.016	−7.947	−7.947	Kuba
$SrZrO_3$	89354	−3.701	0.03	−8.273	−8.273	Kuba
UO_3	26673	−3.212	0.003	−9.628	−9.628	Kuba
Pb_2SiO_4	26343	−2.079	0.011	−6.525	−6.525	NIST
$SiSr_2O_4$	36041	−3.446	0.005	−7.114	−7.114	Kuba
$SiZn_2O_4$	2425	−2.465	0.005	−6.015	−6.015	Kuba
$SiZrO_4$	31130	−3.524	0.011	−8.73	−8.73	NIST
Sr_2TiO_4	20293	−3.426	0.014	−7.436	−7.436	Kuba
P_2O_5	40865	−2.257	0.011	−7.011	−7.011	Kuba
V_2O_5	41030	−2.328	0.003	−7.479	−8.385	Kuba

APPENDIX D

Table IX gives all reactions considered in our data set with their associated experimental and computed reaction energies at 0 K.

TABLE IX. Computed reaction energies with GGA + U, experimental reaction energies (at 0 K) and their difference.

Reaction	Computed reaction energy GGA + U (eV/atom)	Expt. reaction energy (eV/atom)	Difference (eV/atom)
$CaO + MoO_3 \rightarrow CaMoO_4$	−0.281	−0.288	0.007
$TiO_2 + PbO \rightarrow PbTiO_3$	−0.036	−0.065	0.029
$PbO + SiO_2 \rightarrow PbSiO_3$	−0.055	−0.029	−0.025
$SeO_2 + PbO \rightarrow PbSeO_3$	−0.177	−0.195	0.018
$PbO + MoO_3 \rightarrow MoPbO_4$	−0.154	−0.156	0.002
$2PbO + SiO_2 \rightarrow Pb_2SiO_4$	−0.037	−0.041	0.003
$TiO_2 + NiO \rightarrow NiTiO_3$	−0.035	−0.037	0.001
$NiO + SeO_2 \rightarrow NiSeO_3$	−0.099	−0.212	0.113
$NiO + Cr_2O_3 \rightarrow Cr_2NiO_4$	−0.005	−0.004	−0.002
$SiO_2 + 2NiO \rightarrow Ni_2SiO_4$	−0.024	−0.014	−0.010
$0.5Na_2O + 0.5P_2O_5 \rightarrow NaPO_3$	−0.514	−0.536	0.022
$0.5Fe_2O_3 + 0.5Na_2O \rightarrow FeNaO_2$	−0.255	−0.203	−0.051
$0.5Cr_2O_3 + 0.5Na_2O \rightarrow CrNaO_2$	−0.256	−0.261	0.005
$0.5B_2O_3 + 0.5Na_2O \rightarrow BNaO_2$	−0.327	−0.340	0.013
$0.5Na_2O + 1.5B_2O_3 \rightarrow B_3NaO_5$	−0.216	−0.207	−0.010
$0.5Al_2O_3 + 0.5Na_2O \rightarrow AlNaO_2$	−0.258	−0.227	−0.031
$2Na_2O + V_2O_5 \rightarrow Na_4V_2O_7$	−0.432	−0.434	0.003
$2Na_2O + SiO_2 \rightarrow Na_4SiO_4$	−0.354	−0.409	0.056
$P_2O_5 + 2Na_2O \rightarrow Na_4P_2O_7$	−0.645	−0.659	0.014
$0.5P_2O_5 + 1.5Na_2O \rightarrow Na_3PO_4$	−0.658	−0.697	0.039
$Na_2O + UO_3 \rightarrow Na_2UO_4$	−0.348	−0.366	0.017
$3TiO_2 + Na_2O \rightarrow Na_2Ti_3O_7$	−0.201	−0.201	0.000
$Na_2O + SiO_2 \rightarrow Na_2SiO_3$	−0.359	−0.404	0.046
$2SiO_2 + Na_2O \rightarrow Na_2Si_2O_5$	−0.256	−0.270	0.015
$Na_2O + MoO_3 \rightarrow MoNa_2O_4$	−0.468	−0.454	−0.014
$Na_2O + 2MoO_3 \rightarrow Mo_2Na_2O_7$	−0.346	−0.428	0.082
$Na_2O + CrO_3 \rightarrow CrNa_2O_4$	−0.520	−0.492	−0.029
$4B_2O_3 + Na_2O \rightarrow B_8Na_2O_{13}$	−0.184	−0.175	−0.009
$Na_2O + 2B_2O_3 \rightarrow B_4Na_2O_7$	−0.260	−0.249	−0.011
$TiO_2 + MnO \rightarrow MnTiO_3$	−0.086	−0.062	−0.025
$SiO_2 + MnO \rightarrow MnSiO_3$	−0.042	−0.052	0.010

TABLE IX. *(Continued.)*

Reaction	Computed reaction energy GGA + U (eV/atom)	Expt. reaction energy (eV/atom)	Difference (eV/atom)
$0.5MoO_2 + 0.5MoO_3 + 0.5Mn_2O_3 \rightarrow MnMoO_4$	−0.049	−0.084	0.034
$0.67Fe_3O_4 + 0.33Mn_3O_4 \rightarrow Fe_2MnO_4$	−0.016	−0.029	0.014
$2MnO + TiO_2 \rightarrow Mn_2TiO_4$	−0.064	−0.054	−0.010
$SiO_2 + 2MnO \rightarrow Mn_2SiO_4$	−0.067	−0.074	0.007
$V_2O_5 + MgO \rightarrow MgV_2O_6$	−0.064	−0.056	−0.007
$UO_3 + MgO \rightarrow MgUO_4$	−0.030	−0.054	0.024
$MgO + TiO_2 \rightarrow MgTiO_3$	−0.068	−0.055	−0.013
$MgO + 2TiO_2 \rightarrow MgTi_2O_5$	−0.061	−0.027	−0.033
$SiO_2 + MgO \rightarrow MgSiO_3$	−0.053	−0.075	0.022
$MoO_3 + MgO \rightarrow MgMoO_4$	−0.136	−0.095	−0.040
$GeO_2 + MgO \rightarrow GeMgO_3$	−0.063	−0.057	−0.007
$MgO + Cr_2O_3 \rightarrow Cr_2MgO_4$	−0.071	−0.060	−0.011
$Al_2O_3 + MgO \rightarrow Al_2MgO_4$	−0.057	−0.036	−0.021
$3MgO + P_2O_5 \rightarrow Mg_3P_2O_8$	−0.350	−0.347	−0.003
$2MgO + V_2O_5 \rightarrow Mg_2V_2O_7$	−0.113	−0.078	−0.035
$2MgO + SiO_2 \rightarrow Mg_2SiO_4$	−0.079	−0.093	0.014
$0.5P_2O_5 + 0.5Li_2O \rightarrow LiPO_3$	−0.386	−0.422	0.035
$0.5Li_2O + 0.5B_2O_3 \rightarrow BLiO_2$	−0.213	−0.219	0.005
$0.5Al_2O_3 + 0.5Li_2O \rightarrow AlLiO_2$	−0.149	−0.138	−0.011
$Li_2O + ZrO_2 \rightarrow Li_2ZrO_3$	−0.099	−0.116	0.017
$TiO_2 + Li_2O \rightarrow Li_2TiO_3$	−0.221	−0.222	0.001
$Li_2O + SiO_2 \rightarrow Li_2SiO_3$	−0.225	−0.242	0.017
$Li_2O + 2B_2O_3 \rightarrow B_4Li_2O_7$	−0.172	−0.175	0.003
$0.5La_2O_3 + 0.5P_2O_5 \rightarrow LaPO_4$	−0.473	−0.579	0.106
$0.5Al_2O_3 + 0.5La_2O_3 \rightarrow AlLaO_3$	−0.072	−0.121	0.049
$0.5K_2O + 0.5Fe_2O_3 \rightarrow FeKO_2$	−0.234	−0.251	0.016
$0.5K_2O + 0.5B_2O_3 \rightarrow BKO_2$	−0.432	−0.457	0.025
$SiO_2 + K_2O \rightarrow K_2SiO_3$	−0.421	−0.470	0.049
$4SiO_2 + K_2O \rightarrow K_2Si_4O_9$	−0.212	−0.215	0.003
$K_2O + 2SiO_2 \rightarrow K_2Si_2O_5$	−0.317	−0.373	0.055
$CrO_3 + K_2O \rightarrow CrK_2O_4$	−0.676	−0.653	−0.023
$K_2O + 2B_2O_3 \rightarrow B_4K_2O_7$	−0.334	−0.335	0.000
$HgO + SeO_2 \rightarrow HgSeO_3$	−0.100	−0.107	0.006
$SeO_2 + CdO \rightarrow CdSeO_3$	−0.178	−0.194	0.016
$CaO + ZrO_2 \rightarrow CaZrO_3$	−0.059	−0.072	0.013
$CaO + V_2O_5 \rightarrow CaV_2O_6$	−0.182	−0.167	−0.016
$UO_3 + CaO \rightarrow CaUO_4$	−0.182	−0.238	0.056
$TiO_2 + CaO \rightarrow CaTiO_3$	−0.159	−0.171	0.012
$SiO_2 + CaO \rightarrow CaSiO_3$	−0.171	−0.186	0.014
$Nb_2O_5 + CaO \rightarrow CaNb_2O_6$	−0.117	−0.163	0.046
$CaO + GeO_2 \rightarrow CaGeO_3$	−0.148	−0.149	0.001
$CaO + Fe_2O_3 \rightarrow CaFe_2O_4$	−0.053	−0.035	−0.018
$Cr_2O_3 + CaO \rightarrow CaCr_2O_4$	−0.070	−0.090	0.020
$CuO + Cr_2O_3 \rightarrow Cr_2CuO_4$	−0.003	−0.005	0.002
$2FeO + SiO_2 \rightarrow Fe_2SiO_4$	−0.057	−0.020	−0.037
$Al_2O_3 + FeO \rightarrow Al_2FeO_4$	−0.038	−0.027	−0.011
$Cr_2O_3 + FeO \rightarrow Cr_2FeO_4$	−0.072	−0.058	−0.014
$0.5MoO_2 + 0.5MoO_3 + 0.5Fe_2O_3 \rightarrow FeMoO_4$	0.020	0.006	0.014
$TiO_2 + FeO \rightarrow FeTiO_3$	−0.049	−0.043	−0.006
$0.5B_2O_3 + 0.5Rb_2O \rightarrow BRbO_2$	−0.450	−0.440	−0.010
$SiO_2 + ZrO_2 \rightarrow SiZrO_4$	−0.019	−0.026	0.006
$ZnO + SeO_2 \rightarrow SeZnO_3$	−0.093	−0.156	0.063
$ZnO + Fe_2O_3 \rightarrow Fe_2ZnO_4$	−0.033	−0.007	−0.026
$ZnO + Cr_2O_3 \rightarrow Cr_2ZnO_4$	−0.076	−0.092	0.016
$Al_2O_3 + ZnO \rightarrow Al_2ZnO_4$	−0.062	−0.065	0.003
$2ZnO + SiO_2 \rightarrow SiZn_2O_4$	−0.028	−0.046	0.018
$ZrO_2 + SrO \rightarrow SrZrO_3$	−0.142	−0.162	0.019

TABLE IX. *(Continued.)*

Reaction	Computed reaction energy GGA + U (eV/atom)	Expt. reaction energy (eV/atom)	Difference (eV/atom)
$TiO_2 + SrO \rightarrow SrTiO_3$	−0.244	−0.280	0.036
$SrO + SiO_2 \rightarrow SiSrO_3$	−0.257	−0.270	0.013
$SrO + MoO_3 \rightarrow MoSrO_4$	−0.384	−0.365	−0.019
$SrO + HfO_2 \rightarrow HfSrO_3$	−0.169	−0.153	−0.016
$Al_2O_3 + SrO \rightarrow Al_2SrO_4$	−0.132	−0.106	−0.026
$TiO_2 + 2SrO \rightarrow Sr_2TiO_4$	−0.205	−0.236	0.031
$2SrO + SiO_2 \rightarrow SiSr_2O_4$	−0.268	−0.307	0.039
$0.5Cs_2O + 0.5B_2O_3 \rightarrow BCsO_2$	−0.411	−0.435	0.024
$Cs_2O + UO_3 \rightarrow Cs_2UO_4$	−0.448	−0.530	0.082
$Cs_2O + MoO_3 \rightarrow Cs_2MoO_4$	−0.574	−0.630	0.056
$Cs_2O + CrO_3 \rightarrow CrCs_2O_4$	−0.705	−0.736	0.031
$TiO_2 + CoO \rightarrow CoTiO_3$	−0.062	−0.052	−0.010
$CoO + SeO_2 \rightarrow CoSeO_3$	−0.134	−0.237	0.103
$Cr_2O_3 + CoO \rightarrow CoCr_2O_4$	−0.085	−0.087	0.002
$SiO_2 + 2CoO \rightarrow Co_2SiO_4$	−0.030	−0.018	−0.012
$0.5Cr_2O_3 + 0.5Ce_2O_3 \rightarrow CeCrO_3$	−0.039	−0.135	0.097
$0.5Al_2O_3 + 0.5Ce_2O_3 \rightarrow AlCeO_3$	0.004	−0.130	0.135
$ZrO_2 + BaO \rightarrow BaZrO_3$	−0.221	−0.257	0.036
$UO_3 + BaO \rightarrow BaUO_4$	−0.315	−0.378	0.063
$BaO + TiO_2 \rightarrow BaTiO_3$	−0.287	−0.320	0.033
$SiO_2 + BaO \rightarrow BaSiO_3$	−0.297	−0.328	0.031
$MoO_3 + BaO \rightarrow BaMoO_4$	−0.457	−0.384	−0.073
$BaO + Al_2O_3 \rightarrow Al_2BaO_4$	−0.193	−0.152	−0.040
$3BaO + Al_2O_3 \rightarrow Al_2Ba_3O_6$	−0.165	−0.181	0.017
$TiO_2 + 2BaO \rightarrow Ba_2TiO_4$	−0.298	−0.287	−0.011
$2BaO + SiO_2 \rightarrow Ba_2SiO_4$	−0.352	−0.392	0.039
$CrO_3 + Ag_2O \rightarrow Ag_2CrO_4$	−0.145	−0.156	0.012
$SiO_2 + Al_2O_3 \rightarrow Al_2SiO_5$	0.006	−0.011	0.017
$Al_2O_3 + TiO_2 \rightarrow Al_2TiO_5$	0.001	0.015	−0.014
$0.5P_2O_5 + 0.5Al_2O_3 \rightarrow AlPO_4$	−0.270	−0.248	−0.021
$2BeO + SiO_2 \rightarrow Be_2SiO_4$	−0.009	0.017	−0.026
$Al_2O_3 + BeO \rightarrow Al_2BeO_4$	−0.019	−0.024	0.005
$BeO + 3Al_2O_3 \rightarrow Al_6BeO_{10}$	−0.007	0.007	−0.014
$2CaO + B_2O_3 \rightarrow B_2Ca_2O_5$	−0.213	−0.209	−0.004
$Fe_2O_3 + 2CaO \rightarrow Ca_2Fe_2O_5$	−0.071	−0.050	−0.020
$2CaO + P_2O_5 \rightarrow Ca_2P_2O_7$	−0.467	−0.529	0.062
$SiO_2 + 2CaO \rightarrow Ca_2SiO_4$	−0.192	−0.219	0.027
$V_2O_5 + 2CaO \rightarrow Ca_2V_2O_7$	−0.252	−0.249	−0.003
$3CaO + P_2O_5 \rightarrow Ca_3P_2O_8$	−0.496	−0.564	0.068
$Al_2O_3 + 3CaO \rightarrow Al_2Ca_3O_6$	−0.035	−0.013	−0.021
$B_2O_3 + 3CaO \rightarrow B_2Ca_3O_6$	−0.213	−0.234	0.021
$2SiO_2 + 3CaO \rightarrow Ca_3Si_2O_7$	−0.181	−0.188	0.007
$3CaO + V_2O_5 \rightarrow Ca_3V_2O_8$	−0.220	−0.260	0.041
$3TiO_2 + 4CaO \rightarrow Ca_4Ti_3O_{10}$	−0.137	−0.185	0.048
$CaO + Al_2O_3 \rightarrow Al_2CaO_4$	−0.061	−0.027	−0.034
$2Al_2O_3 + CaO \rightarrow Al_4CaO_7$	−0.057	−0.015	−0.042
$CaO + B_2O_3 \rightarrow B_2CaO_4$	−0.186	−0.178	−0.008
$2B_2O_3 + CaO \rightarrow B_4CaO_7$	−0.142	−0.136	−0.007

---

[*] Current address: Institut de la Matière Condensée et des Nanosciences (IMCN)-Nanoscopic Physics (NAPS), Université Catholique de Louvain.

[†] gceder@mit.edu

[1] G. Ceder, G. Hautier, A. Jain, and S. P. Ong, MRS Bulletin **36**, 185 (2011).

[2] A. R. Akbarzadeh, C. Wolverton, and V. Ozolins, Phys. Rev. B **79**, 184102 (2009).

[3] S. V. Alapati, J. Karl Johnson, and D. S. Sholl, PhysChemChemPhys **9**, 1438 (2007).

[4] A. Jain, S.-A. Seyed-Reihani, C. C. Fischer, D. J. Couling, G. Ceder, and W. H. Green, Chem. Eng. Sci. **65**, 3025 (2010).

[5] Y. Duan and D. C. Sorescu, J. Chem. Phys. **133**, 074508 (2010).

[6] B. Meredig and C. Wolverton, Phys. Rev. B **80**, 245119 (2009).

[7] Y. Duan, B. Zhang, D. C. Sorescu, and J. K. Johnson, J. Solid State Chem. **184**, 304 (2011).

[8] M. van Setten, G. de Wijs, V. Popa, and G. Brocks, Phys. Rev. B **72**, 073107 (2005).

[9] L. Wang, T. Maxisch, and G. Ceder, Chem. Mater. **19**, 543 (2007).

[10] S. P. Ong, L. Wang, B. Kang, and G. Ceder, Chem. Mater. **20**, 1798 (2008).

[11] S. P. Ong, A. Jain, G. Hautier, B. Kang, and G. Ceder, Electrochem. Comm. **12**, 427 (2010).

[12] J. C. Kim, C. J. Moore, B. Kang, G. Hautier, A. Jain, and G. Ceder, J. Electrochem. Soc. **158**, A309 (2011).

[13] R. E. Doe, K. A. Persson, Y. S. Meng, and G. Ceder, Chem. Mater. **20**, 5274 (2008).

[14] R. E. Doe, K. A. Persson, G. Hautier, and G. Ceder, Electrochem. Solid State Lett. **12**, A125 (2009).

[15] A. N. Kolmogorov, M. Calandra, and S. Curtarolo, Phys. Rev. B **78**, 094520 (2008).

[16] O. Levy, R. V. Chepulskii, G. L. W. Hart, and S. Curtarolo, J. Am. Chem. Soc. **132**, 833 (2010).

[17] A. Kolmogorov, S. Shah, E. Margine, A. Bialon, T. Hammerschmidt, and R. Drautz, Phys. Rev. Lett. **105**, 217003 (2010).

[18] G. Hautier, C. C. Fischer, A. Jain, T. Mueller, and G. Ceder, Chem. Mater. **22**, 3762 (2010).

[19] X. Zhang, A. Zunger, and G. Trimarchi, J. Chem. Phys. **133**, 194504 (2010).

[20] G. Hautier, A. Jain, S. P. Ong, B. Kang, C. Moore, R. Doe, and G. Ceder, Chem. Mater. **23**, 3945 (2011).

[21] T. Mueller, G. Hautier, A. Jain, and G. Ceder, Chem. Mater. **23**, 3854 (2011).

[22] G. Hautier, A. Jain, H. Chen, C. Moore, S. P. Ong, and G. Ceder, J. Mater. Chem. **21**, 17147 (2011).

[23] G. Jóhannesson, T. Bligaard, A. Ruban, H. Skriver, K. Jacobsen, and J. Nørskov, Phys. Rev. Lett. **88**, 255506 (2002).

[24] J. Feng, R. G. Hennig, N. W. Ashcroft, and R. Hoffmann, Nature (London) **451**, 445 (2008).

[25] J. von Appen and R. Dronskowski, Angew. Chem., Int. Ed. **44**, 1205 (2005).

[26] D. Fredeman, P. Tobash, M. Torrez, J. Thompson, E. Bauer, F. Ronning, W. Tipton, S. Rudin, and R. Hennig, Phys. Rev. B **83**, 224102 (2011).

[27] I. E. Castelli, T. Olsen, S. Datta, D. D. Landis, S. Dahl, K. S. Thygesen, and K. W. Jacobsen, Energy Environ. Sci. **5**, 5814 (2012).

[28] F. Calle-Vallejo, J. I. Martínez, J. M. García-Lastra, M. Mogensen, and J. Rossmeisl, Angew. Chem., Int. Ed. **49**, 7699 (2010).

[29] J.-R. Martinez, C. E. Mohn, S. Stølen, and R. Søndenå, PhysChemChemPhys **8**, 2036 (2006).

[30] L. A. Curtiss, K. Raghavachari, G. W. Trucks, and J. A. Pople, J. Chem. Phys. **94**, 7221 (1991).

[31] L. A. Curtiss, K. Raghavachari, P. C. Redfern, V. Rassolov, and J. A. Pople, J. Chem. Phys. **109**, 7764 (1998).

[32] O. Kubaschewski, C. B. Alcock, and P. J. Spencer, *Materials Thermochemistry*, 6th ed. (Pergamon, New York, 1993), Chap. 5, pp. 257–323.

[33] M. W. Chase, *NIST-JANAF Thermochemical Tables* (American Institute of Physics, Woodbury, NY, 1998).

[34] J. Perdew, K. Burke, and M. Ernzerhof, Phys. Rev. Lett. **77**, 3865 (1996).

[35] V. I. Anisimov, J. Zaanen, and O. K. Andersen, Phys. Rev. B **44**, 943 (1991).

[36] V. I. Anisimov, F. Aryasetiawan, and A. I. Lichtenstein, J. Phys.: Condens. Matter **9**, 767 (1997).

[37] L. Wang, T. Maxisch, and G. Ceder, Phys. Rev. B **73**, 195107 (2006).

[38] G. Kresse and J. Furthmuller, Comput. Mater. Sci. **6**, 15 (1996).

[39] P. E. Blöchl, Phys. Rev. B **50**, 17953 (1994).

[40] A. Jain, G. Hautier, C. J. Moore, S. P. Ong, C. C. Fischer, T. Mueller, K. A. Persson, and G. Ceder, Comput. Mater. Sci. **50**, 2295 (2011).

[41] G. L. W. Hart and R. W. Forcade, Phys. Rev. B **77**, 224115 (2008).

[42] W. Setyawan and S. Curtarolo, Comput. Mater. Sci. **49**, 299 (2010).

[43] W. Setyawan, R. M. Gaume, S. Lam, R. S. Feigelson, and S. Curtarolo, ACS Comb. Sci. **13**, 382 (2011).

[44] ICSD, *Inorganic Crystal Structure Database* (2006).

[45] Thermochemistry, *Landolt-Bornstein Database* (2011).

[46] [http://www.ctdp.org/].

[47] E. G. King, J. Phys. Chem. **60**, 410 (1956).

[48] X. Ke, A. Kuwabara, and I. Tanaka, Phys. Rev. B **71**, 184107 (2005).

[49] Z.-g. Mei, Y. Wang, S.-l. Shang, and Z.-k. Liu, Inorg. Chem. **50**, 6996 (2011).

[50] See Supplemental Material at http://link.aps.org/supplemental/10.1103/PhysRevB.85.155208 for cif files of the GGA($+U$) relaxed structure in their fm state.

[51] C. Franchini, R. Podloucky, J. Paier, M. Marsman, and G. Kresse, Phys. Rev. B **75**, 195128 (2007).

[52] S. Lany, Phys. Rev. B **78**, 245207 (2008).

[53] D. G. Pettifor, J. Chem. Soc., Faraday Trans. **86**, 1209 (1990).

[54] N. Skorodumova, R. Ahuja, S. Simak, I. Abrikosov, B. Johansson, and B. Lundqvist, Phys. Rev. B **64**, 115108 (2001).

[55] C. Loschen, J. Carrasco, K. Neyman, and F. Illas, Phys. Rev. B **75**, 035115 (2007).

[56] R. Ahuja, A. Blomqvist, P. Larsson, P. Pyykkö, and P. Zaleski-Ejgierd, Phys. Rev. Lett. **106**, 018301 (2011).

[57] T. Lindemer, T. Besmann, and C. Johnson, J. Nucl. Mater. **100**, 178 (1981).

[58] T. Mathews, D. Krishnamurthy, and T. Gnanasekaran, J. Nucl. Mater. **247**, 280 (1997).

[59] P. A. G. O'Hare, J. Chem. Thermodyn. **6**, 425 (1974).

[60] N. K. Shukla, R. Prasad, and D. D. Sood, J. Chem. Thermodynamics **25**, 429 (1993).

[61] Z. Singh, S. Dash, and R. Prasad, J. Alloys Compd. **279**, 287 (1998).

[62] A. Olin, *Chemical Thermodynamics of Selenium*, Vol. 1 (Elsevier, Amsterdam, 2005).

[63] Y. Tardy and P. Vieillard, Contrib. Mineral. Petrol. **63**, 75 (1977).

[64] S. R. Eliason, *Maximum Likelihood Estimation: Logic and Practice* (Sage Publications, London, 1993).

[65] B. Efron and D. Hinkely, Biometrika **65**, 457 (1978).

[66] For instance, we found during our investigation that the “Mo” PAW pseudopotentials provided by VASP led to much larger errors for some reaction energies (e.g., $Na_2O + MoO_3 \rightarrow Na_2MoO_4$) than if the “Mo_$pv$” pseudopotential, including the p electrons as valence electrons, was used.

[67] [http://www.materialsproject.org/].
[68] A. Jain, G. Hautier, S. P. Ong, C. J. Moore, C. C. Fischer, K. A. Persson, and G. Ceder, Phys. Rev. B **84**, 045115 (2011).
[69] Y. Mo, S. Ong, and G. Ceder, Phys. Rev. B **84**, 205446 (2011).
[70] J. Heyd, G. E. Scuseria, and M. Ernzerhof, J. Chem. Phys. **118**, 8207 (2003).
[71] R. Armiento and A. Mattsson, Phys. Rev. B **72**, 085108 (2005).
[72] A. Mattsson and R. Armiento, Phys. Rev. B **79**, 155101 (2009).
[73] V. L. Chevrier, S. P. Ong, R. Armiento, M. K. Y. Chan, and G. Ceder, Phys. Rev. B **82**, 075122 (2010).
[74] W. Foulkes, L. Mitas, R. Needs, and G. Rajagopal, Rev. Mod. Phys. **73**, 33 (2001).
[75] Debye temperature, heat capacity, density, melting and boiling points, Landolt-Bornstein Database (2011).
[76] H. Flotow and D. Osborne, J. Chem. Thermodyn. **6**, 135 (1974).
[77] S. Stolen, R. Glockner, F. Gronvold, A. Tooru, and S. Izumisawa, Am. Mineral. **81**, 973 (1996).